ORTA DOĞU TEKNİK ÜNİVERSİTESİ
FEN BİLİMLERİ ENSTİTÜSÜ MÜDÜRLÜĞÜ

TEZ ŞABLONU ONAY FORMU
THESIS TEMPLATE CONFIRMATION FORM

1. Şablonda verilen yerleşim ve boşluklar değiştirilmemelidir.
2. **Jüri tarihi** Başlık Sayfası, İmza Sayfası, Abstract ve Öz'de ilgili yerlere yazılmalıdır.
3. İmza sayfasında jüri üyelerinin unvanları doğru olarak yazılmalıdır. Tüm imzalar **mavi pilot kalemle** atılmalıdır.
4. **Disiplinlerarası** programlarda görevlendirilen öğretim üyeleri için jüri üyeleri kısmında tam zamanlı olarak çalıştıkları anabilim dalı başkanlığının ismi yazılmalıdır. Örneğin: bir öğretim üyesi Biyoteknoloji programında görev yapıyor ve biyoloji bölümünde tam zamanlı çalışıyorsa, İmza sayfasına biyoloji bölümü yazılmalıdır. İstisnai olarak, disiplinler arası program başkanı ve tez danışmanı için disiplinlerarası program adı yazılmalıdır.
5. Tezin **son sayfasının sayfa** numarası Abstract ve Öz'de ilgili yerlere yazılmalıdır.
6. Bütün chapterlar, referanslar, ekler ve CV sağ sayfada başlamalıdır. Bunun için **kesmeler** kullanılmıştır. **Kesmelerin kayması** fazladan boş sayfaların oluşmasına sebep olabilir. Bu gibi durumlarda paragraf (¶) işaretine tıklayarak kesmeleri görünür hale getirin ve yerlerini **kontrol edin**.
7. Figürler ve tablolar kenar boşluklarına taşmamalıdır.
8. Şablonda yorum olarak eklenen uyarılar dikkatle okunmalı ve uygulanmalıdır.
9. Tez yazdırılmadan önce PDF olarak kaydedilmelidir. Şablonda yorum olarak eklenen uyarılar PDF dokümanında yer almamalıdır.
10. Tez taslaklarının kontrol işlemleri tamamlandığında, bu durum öğrencilere METU uzantılı öğrenci e-posta adresleri aracılığıyla duyurulacaktır.
11. Tez yazım süreci ile ilgili herhangi bir sıkıntı yaşarsanız, Sıkça Sorulan Sorular (SSS) sayfamızı ziyaret ederek yaşadığınız sıkıntıyla ilgili bir çözüm bulabilirsiniz.

1. Do not change the spacing and placement in the template.
2. Write **defense date** to the related places given on Title page, Approval page, Abstract and Öz.
3. Write the titles of the examining committee members correctly on Approval Page. **Blue ink** must be used for all signatures.
4. For faculty members working in **interdisciplinary programs**, the name of the department that they work full-time should be written on the Approval page. For example, if a faculty member staffs in the biotechnology program and works full-time in the biology department, the department of biology should be written on the approval page. Exceptionally, for the interdisciplinary program chair and your thesis supervisor, the interdisciplinary program name should be written.
5. Write **the page number of the last page** in the related places given on Abstract and Öz pages.
6. All chapters, references, appendices and CV must be started on the right page. **Section Breaks** were used for this. **Change in the placement** of section breaks can result in extra blank pages. In such cases, make the section breaks visible by clicking paragraph (¶) mark and **check their position.**
7. All figures and tables must be given inside the page. Nothing must appear in the margins.
8. All the warnings given on the comments section through the thesis template must be read and applied.
9. Save your thesis as pdf and Disable all the comments before taking the printout.
10. This will be announced to the students via their METU students e-mail addresses when the control of the thesis drafts has been completed.
11. If you have any problems with the thesis writing process, you may visit our Frequently Asked Questions (FAQ) page and find a solution to your problem.

☒ **Yukarıda bulunan tüm maddeleri okudum, anladım ve kabul ediyorum. / I have read, understand and accept all of the items above.**

Name : **Mert**
Surname : **Top**
E-Mail : **mert.top@metu.edu.tr**
Date :
Signature : _____

TESTING, MODELLING AND SIMULATION OF LINEAR AND CIRCULAR LINEAR SHAPED CHARGES

A THESIS SUBMITTED TO
THE GRADUATE SCHOOL OF NATURAL AND APPLIED SCIENCES
OF
MIDDLE EAST TECHNICAL UNIVERSITY

BY

MERT TOP

IN PARTIAL FULFILLMENT OF THE REQUIREMENTS
FOR
THE DEGREE OF MASTER OF SCIENCE
IN
MECHANICAL ENGINEERING

JULY 2022

Approval of the thesis:

TESTING, MODELLING AND SIMULATION OF LINEAR AND CIRCULAR LINEAR SHAPED CHARGES

submitted by **MERT TOP** in partial fulfillment of the requirements for the degree of **Master of Science** i**n Mechanical Engineering, Middle East Technical University** by,

Prof. Dr. Halil Kalıpçılar
Dean, Graduate School of **Natural and Applied Sciences** _____

Prof. Dr. M. A. Sahir Arıkan
Head of the Department, **Mechanical Engineering** _____

Assoc. Prof. Dr. Hüsnü Dal
Supervisor, **Mechanical Engineering, METU** _____

Prof. Dr. R. Orhan Yıldırım
Co-Supervisor, **Mechanical Engineering, METU** _____

Examining Committee Members:

Assoc. Prof. Dr. Ali Emre Turgut
Mechanical Engineering, METU _____

Assoc. Prof. Dr. Hüsnü Dal
Mechanical Engineering, METU _____

Prof. Dr. Ömer Anlağan
Mechanical Engineering, Bilkent University _____

Assist. Prof. Dr. Orkun Özşahin
Mechanical Engineering, METU _____

Assist. Prof. Dr. Hakan Çalışkan
Mechanical Engineering, METU _____

Date: 28.07.2022

I hereby declare that all information in this document has been obtained and presented in accordance with academic rules and ethical conduct. I also declare that, as required by these rules and conduct, I have fully cited and referenced all material and results that are not original to this work.

Name Last name : Mert Top

Signature :

ABSTRACT

TESTING, MODELLING AND SIMULATION OF LINEAR AND CIRCULAR LINEAR SHAPED CHARGES

Top, Mert
Master of Science, Mechanical Engineering
Supervisor: Assoc. Prof. Dr. Hüsnü Dal
Co-Supervisor: Prof. Dr. R. Orhan Yıldırım

July 2022, 85 pages

In this thesis, testing, modelling, and simulation studies of the Linear Shaped Charge (LSC) and Circular Linear Shaped Charge (CLSC) are presented.

CLSC is an alternative design to the Flexible Linear Shaped Charge (FLSC). It contains a copper liner and metal housing which are designed and produced by considering the target profile. Then, a molten explosive (PBX-110) is cured inside the copper and housing, so the CLSC production is completed. By following this production method, different LSC and CLSC configurations are produced and tested for different target geometries. For each configuration, parameters that affect the penetration efficiency are investigated. Sufficient penetration results are obtained which can be an alternative to a FLSC penetration.

Furthermore, an analytical and numerical model is developed to simulate the LSC and CLSC experiments. In the analytical model, a MATLAB code which calculates jet formation and target penetration is written by using theoretical formulas. In the numerical model, a 2D AUTODYN model is created. Jet formation and target

penetration of the LSC and CLSC experiments are simulated. Reasonable results are obtained with the experiments for each of the analytical and numerical models.

Keywords: Circular Linear Shaped Charge (CLSC), Linear Shaped Charge (LSC), Jet Formation, Penetration, AUTODYN.

ÖZ

DOĞRUSAL VE DAİRESEL ÇUKUR İMLA TEST, MODELLEME VE SİMÜLASYON ÇALIŞMALARI

Top, Mert
Yüksek Lisans, Makina Mühendisliği
Tez Yöneticisi: Assoc. Prof. Dr. Hüsnü Dal
Ortak Tez Yöneticisi: Prof. Dr. R. Orhan Yıldırım

Temmuz 2022, 85 sayfa

Bu tezde Doğrusal Çukur İmla (DÇİ) ve Dairesel Çukur İmla (DAÇİ) test, modelleme ve simülasyon çalışmaları sunulmaktadır.

Bu çalışmada DAÇİ, BDÇİ'ye alternatif bir ürün olarak tasarlanmıştır. Söz konusu ürün, geometrisi kesilmesi istenilen hedef profiline uygun olarak üretilen birbirine mekanik olarak bağlı bakır astar ve metal gövde içermektedir. Bu yapının içerisine doldurulan döküm patlayıcının içeride kürleştirilmesiyle DAÇİ ürününün üretimi tamamlanmaktadır. Bu üretim metodu takip edilerek kesilmesi hedeflenen farklı hedeflere uygun olarak farklı DÇİ ve DAÇİ konfigürasyonları üretilmiş ve test edilmiştir. Her bir konfigürasyonda, delme derinliğini etkileyen parametreler incelenmiştir. Testler sonucunda BDÇİ ürününe alternatif olabilecek yeterli delme derinlikleri elde edilmiştir.

Çalışmanın devamında yapılan DÇİ ve DAÇİ testlerinin simüle edilmesi için analitik ve numerik modeller geliştirilmiştir. Analitik model, jet oluşumu ve jet penetrasyonunun simüle edilebilmesi için MATLAB programı kullanılarak

oluşturulmuştur. Numerik modelinin geliştirilmesiyse 2 boyutlu olarak AUTODYN programında yapılmıştır. Hem analitik hem de numerik modelle test konfigürasyonları simüle edilmiş ve test sonuçlarına yakın delme derinlikleri elde edilmiştir.

Anahtar Kelimeler: Dairesel Çukur İmla (DAÇİ), Doğrusal Çukur İmla (DÇİ), Jet Oluşumu, Penetrasyon, AUTODYN.

To my family

ACKNOWLEDGMENTS

I would like to express my gratitude and regard to my supervisor Assoc. Prof. Dr. Hüsnü Dal for his understanding and goodwill throughout this work.

I would like to express my deepest thanks to my co-supervisor Prof. Dr. R. Orhan Yıldırım for his great guidance, support, goodwill and interest throughout this study.

I specially would like to thank Hüseyin Altıntaş, Muhammed Yusuf Yılmaz and Yunus Emre Sert for their patience, support and valuable aids.

I also would like to thank to all my friends, superiors and colleagues in ROKETSAN for their patience, support and valuable aids for this work.

I would like to thank to ROKETSAN Missile Industries for their software and hardware support.

TABLE OF CONTENTS

LIST OF TABLES

TABLES

LIST OF FIGURES

FIGURES

NOMENCLATURE

CLSC	Circular Linear Shaped Charge
CH-6	Composition of %97.5 RDX, %1.5 Calcium Stearate, %0.5 Polyisobutylene, and %0.5 Graphite
ETP Copper	Electrolytic Tough Pitch Copper
FLSC	Flexible Linear Shaped Charge
HNS	Hexanitrostilbene
LSC	Linear Shaped Charge
M/C	Liner to Explosive Mass Ratio
OFHC Copper	Oxygen-free Copper
PBX-110	Polymer-bonded Explosive
RDX	Research Department Explosive

LIST OF SYMBOLS

C_1 & C_2	Explosive parameters which can be determined empirically from experiments
D	detonation velocity
l	length of the jet element
L	length of the jet
m_j	mass of the jet element
n	number of elements
P_{cj}	Chapman Jouget pressure
r	initial radius of jet element
R_t	target resistance
t	current time
t_o	initial time
t_s	time step
U	penetration velocity
U_{det}	sweep velocity

V	element jet velocity
V_c	collapse velocity
V_j	jet velocity
V_{pl}	plastic velocity
V_s	slug velocity
V_0	accelerating collapse velocity
V'_0	derivative of the collapse angle with respect to liner height
Y	dynamic yield strength of the liner
Y_p	penetrator resistance
α	experimental constant
β	corrected collapse angle
β^+	steady state collapse angle
γ	angle of incidence
δ	projection angle
μ	liner to mass ratio
ρ	density
τ	time constant

CHAPTER 1

INTRODUCTION

Linear Shaped Charges (LSC) are used very frequently in aerospace and civil industry to cut or demolish targets instantaneously. In aerospace, generally they are used for flight termination of rocket or missile, separation of launch vehicle, cutting of the aircraft canopy during the pilot evacuation by seat ejection system. In civil industry, they are used to demolish big structures such as bridges, cranes, and buildings.

A LSC generally consists of a secondary explosive, a metal liner, a metal sheath or housing. As the explosive inside of the LSC is detonated by a detonator, metal liner melts instantaneously and collapse to symmetry axis of the LSC. By the velocity gradient difference of the liner particles, a long/dense metal jet is formed and penetrate to selected target at supersonic speeds and then cut or demolish it.

There are different types of LSCs which change according to target geometry. Use of LSC is sufficient for straight targets. In this type, liner material of the LSC is generally copper or aluminum which is not flexible. However, if the target geometry is not a straight line, then the LSC should be bendable so that it can take the profile of the target. In such cases, Flexible Linear Shaped Charge (FLSC) is used which contains a flexible metal liner (for example antimonial lead) so the FLSC can be bended according to desired profile, then the target shapes can be cut.

Furthermore, another way of cutting different profiles is designing the LSC parts according to target profile. In this study, different circular profiles are cut by this method. Copper liner and metal housing are designed and produced by considering the target profile. Then, a molten explosive (PBX-110) is cured inside the copper and housing. Finally, the explosive is detonated by a detonator and desired targets

profiles are cut by the prototypes. Designed prototypes are named as Circular Linear Shaped Charge (CLSC).

CLSC has a different design from LSC and FLSC, but since the functioning principle is the same, the analytical theory and numerical hydrocodes are applicable for the CLSC while examining the jet formation and jet penetration. After conducting the CLSC experiments, a MATLAB code which calculate jet formation and target penetration is written by using theoretical formulas. Reasonable penetration results are obtained with experiments. Also, a 2D AUTODYN model is created. Jet formation and target penetration of the CLSC experiments are simulated by using this model. Again, reasonable results are obtained by the experiments.

CHAPTER 2

LITERATURE REVIEW

2.1 Fundamentals of LSC

Functioning of a LSC can be described as with the following phenomena: When the explosive charge detonates, it focuses detonation energy towards a cavity while the shock wave deforms and accelerates the liner. Reverse V geometry of LSC ensures the formation of a long/dense jet which is called ”Munroe Effect” phenomenon [1].

After the formation of the jet, it starts to penetrate on the selected target. Cutting mechanism of the target by the formed jet consists of two principles:

• The primary mechanism is the penetration of the jet of the linear shaped charge into the target material. When the jet reaches the target, the pressure of the jet on the material is significantly larger than the compressive strength of the material. Due to that, the jet penetrates into the target and forms a cut. When kinetic energy of the jet in the process of penetration is reduced to a certain value because of the resistance of the plastically deformed material, which depends on the target material, the penetration stops [1].

• The secondary mechanism is caused by the contribution of the shock waves. If the thickness of the target is slightly greater than penetration, the total penetration of the target may be completed by the cracks which is created by shock waves. On the other hand, if the thickness of the material is sufficiently large, the impact of the shock waves is lowered, and the size of the crack created in that manner is insignificant [1].

The sum of these mechanisms prevails the total penetration of the LSC to the target [1]. Formation of the jet and its penetration into target is given in Figure 2-1.

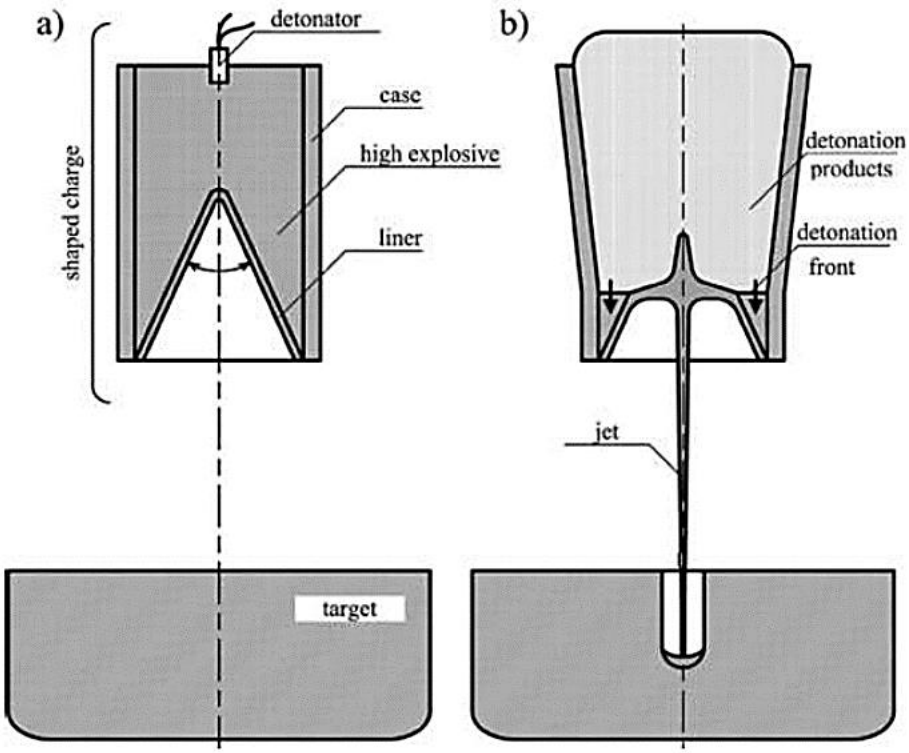

Figure 2-1 Formation of a LSC jet and penetration of it to a target [1]

2.1.1 Factors Affecting the Cutting Performance

There are some important factors which affect the cutting performance of a LSC. These are liner material, liner geometry, liner to explosive mass ratio, stand-off distance and initiation method (especially for large size LSCs).

2.1.1.1 Liner Material

Liner material has a great importance for LSC cutting performance. The long, dense and adherent jet ensures the continuity of the jet and increases the cutting performance [1]. There is a work which ranks the suitability of different metals for the use as liner. Density, bulk sound speed, and the maximum theoretical velocity of jet parameters are analyzed for different materials and ranked in Table 2-1 [2]. But

it should not be forgotten that for this work ease of manufacturability is out of concept.

Table 2-1 Ranking of Different Metals as a Liner Material [2]

Physical properties	Al	Ni	Cu	Mo	Ta	U	W
Density (g/cm^3)	2.7	8.8	8.9	10	16.6	18.5	19.4
Bulk sound speed (km/s)	5.4	4.4	4.3	4.9	2.4	2.5	4
$v_{jt,\max}$ (km/s)	12.3	10.1	9.8	11.3	5.4	5.7	9.2
$v_{jt,\max}\sqrt{\rho_j}$	20.2	30	29.2	35.7	22	22	40.4
Rank	7	3	4	2	6	5	1

Furthermore, selection of liner material differs for LSC design. Copper is generally used as liner material for large explosive mass. Larger explosive mass LSC designs has larger stand-off distances, so the LSC jet should travel larger distances to cut the target. Since copper has higher dynamic yield strength than most of the metals [23], the jet break-up is more likely to occur at a larger distance. Lead is used for LSCs where flexibility and bendability are needed for the product.

2.1.1.2 Liner Geometry

The sheath geometry is another parameter that affects the cutting performance of LSC. The chevron apex height, apex angle and liner thickness are directly affect cutting performance so all these parameters are needed to be studied to design the optimum product [4].

Chevron sheath geometry of LSC is symmetrical. Deviations from this symmetry during production may cause undesirable conditions such as deviation from the target at large stand-off distances, decrease in cutting performance due to angular attacks that will occur which is perpendicular to the material to be cut during firing [1]. Deviation from the symmetry of a LSC is studied by Novetny and Mallery with simulations and experiments [5]. Offsetting laterally the explosive of a LSC (Figure 2-2) results with following penetration deviations (Figure 2-3):

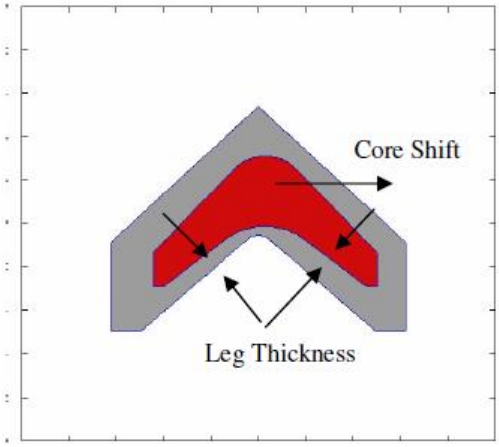

Figure 2-2 Core Offset View [5]

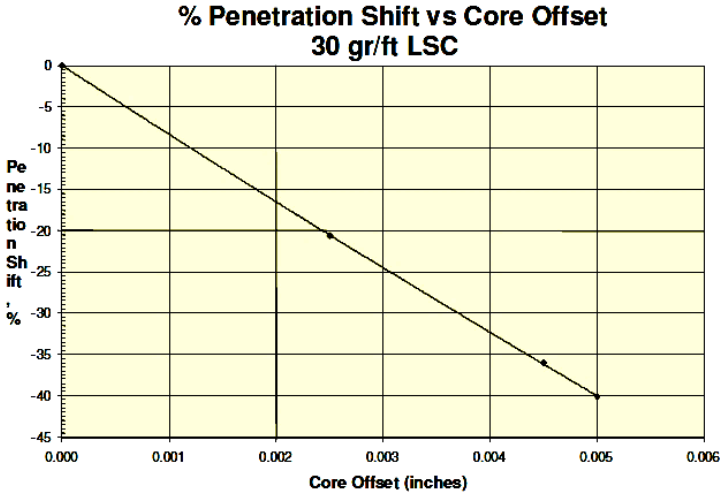

Figure 2-3 % Penetration Shift vs. Core Offset Plot [5]

So, 0.005-inch explosive offset for a 30 gr/ft LSC, may cause %40 loss of penetration. Deviation and loss of penetration can also be observed Figure 2-4.

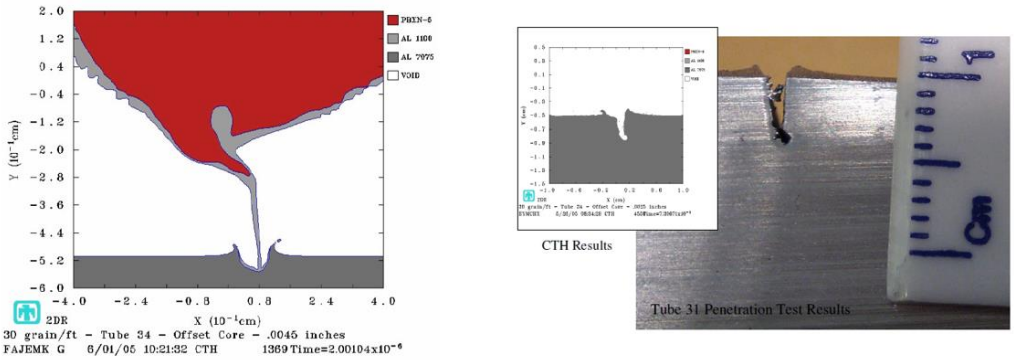

Figure 2-4 Effect of Deviation from Core Offset for LSC [5]

2.1.1.3 Liner to Explosive Mass Ratio

Liner to explosive mass ratio (M/C) is also very important for the penetration efficiency. A relatively high M/C ratio affects the acceleration of the jet and results in a lower jet velocity and lower penetration. For low M/C ratios, after some value, penetration reaches to its saturation point because of the maximum theoretical jet velocity of the liner material. So, optimizing the M/C ratio reveals higher penetrations with lower explosive mass [1, 6].

2.1.1.4 Stand-Off Distance

Stand-off distance is a very important parameter for LSC penetration efficiency. During the functioning of LSC, a pre-optimized distance is needed for liner to accelerate and form the jet [1, 6, 7]. If the target is too close to LSC, before reaching its final velocity and jet length, penetration begins earlier and then the efficiency decreases. On the other hand, if the stand-off distance is too far away, jet break-up begins, and it starts to disperse by deviating from the penetration axis then causing decrease in the penetration efficiency [1, 6, 7]. Effect of stand-off distance to penetration efficiency can easily be seen in Figure 2-5:

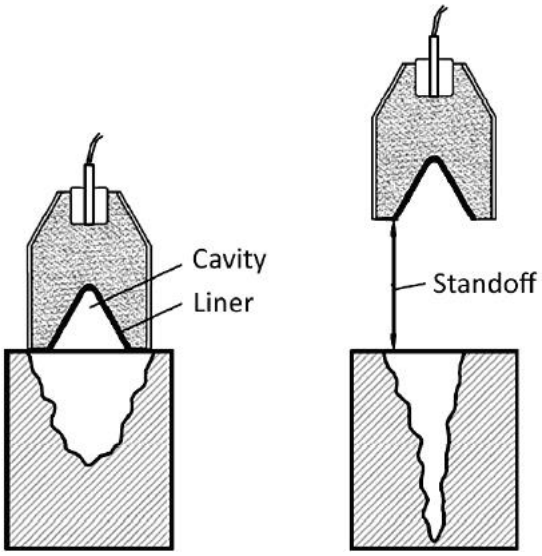

Figure 2-5 Effect of the LSC Stand-Off Distance for the Penetration Efficiency [1]

Optimum stand-off distance is both related with geometrical properties (jet thickness, jet length, apex angle), and mechanical properties of liner and explosive (density, strength). So, the stand-off distance should be optimized when designing a new LSC [1]. Optimum stand-off distances are much smaller for LSCs than those of Shaped Charges. Therefore, it is much less likely to have the formation of jet break-ups for LSC.

2.1.1.5 Initiation Method

Initiation method is very critical for penetration efficiency of the LSC. In a source, it is stated that initiating explosive of the LSC with a low-profile detonator may lead to weak detonations on the main explosives [8]. So, in the case of LSC initiation, penetration efficiency may decrease in such a condition.

In an another source, it is shown by experiments that initiating larger LSCs (which contain high explosive mass) with dual initiation method (two point single end initiation method) increases the penetration efficiency [9]. By using this method, a

planar detonation wave forms and it increases the penetration efficiency especially for the larger LSCs. Dual initation method of a LSC is given in Figure 2-6.

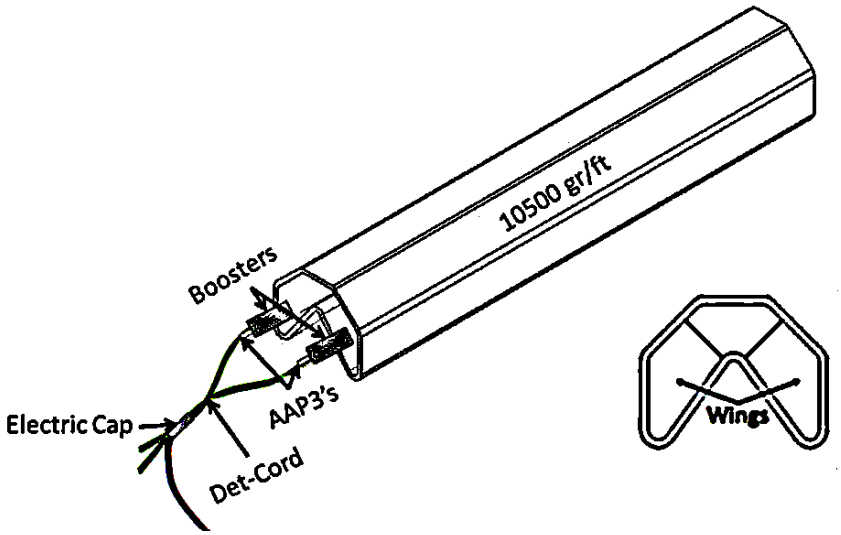

Figure 2-6 Dual Initiation of a High Explosive Mass LSC [9]

2.2 Production Techniques

Type of explosives which is used in production of LSC can be classified as powder form, molten form, and plastic form explosives. According to type of explosive, production techniques and design of the LSCs also change.

2.2.1 Powder Form LSC Production

A LSC which contains powder form explosive can be produced by the following procedure:

a) One side of a metallic tube is buckled.
b) Metallic tube is filled with powder formed explosive. During the filling operation the tube can be vibrated to ensure the fluidity of the explosive inside of the tube [10]. To control the explosive density inside the tube, a tamping rod may also be used; then when filling the explosive, it can be used to compress the explosive periodically [10]. CH-6 explosive is more

preferred for powder form LSC designs for its workability (pressing, rolling, explosive fluency etc.) and insensitivity [11]. Also, HNS (Hexanitrostilbene) is used especially for the space applications since it is thermally more stable at higher temperatures [12].

c) The other side of the tube is buckled.
d) Explosive filled tube is passed in a grooving machine a number of times, by increasing the groove depth on each pass (swage rolling operation) [11, 13].

Especially for the larger LSCs, a pre-rolling operation can be made before fillling the explosive inside the tube. Then, stresses on the tube can be minimized during the rolling operation [10]. Another key point on the operation is that the number of passes from the grooving machine: Forming the groove to its total depth in one pass may cause the casing to split longitudinally at the apex of the groove [13]. So, determining the number of passes are needed for processable designs.

Filling and rolling operations of a LSC can be examined from Figure 2-7 and Figure 2-8:

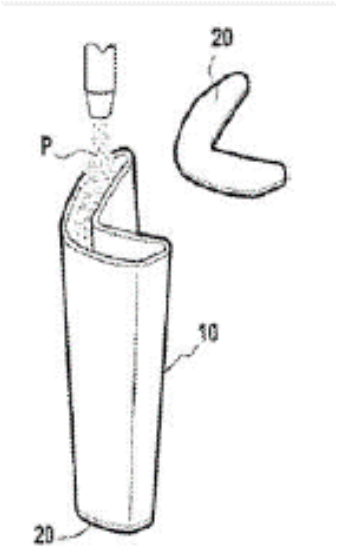

Figure 2-7 Filling of Powder Form Explosive Inside a Pre-rolled Tube [10]

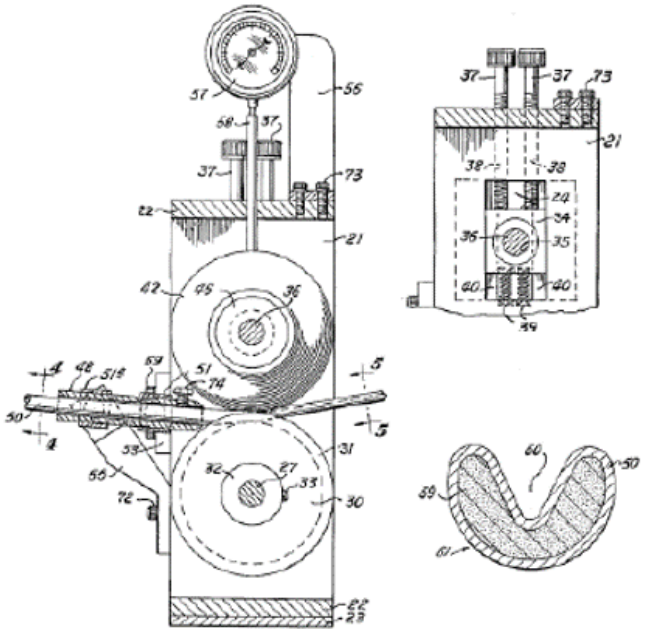

Figure 2-8 Rolling Operation of a Powder Form LSC [13]

In many cases, it is needed to cut different profiles. So, it is needed for LSCs to be bendable and take the form the desired cutting profile. This form of a LSC is called Flexible Linear Shaped Charge (FLSC). Selection of tube material is very important for the bendability of a FLSC. Literature is agreed that use of %5-6 antimonial lead as a tube material ensures FLSC designs with ease of manufacture, reliable performance, circumferential and superficial bendability [4, 11, 13].

2.2.2 Molten Form LSC Production

Another way of producing LSC is to fill a pre-rolled tube with molten explosive and to solidify it by curing [13]. By this method, there is no need of rolling operation on explosive filled LSCs. Therefore, the production process time and the cost decrease significantly. However, if FLSC is needed, bendability of such designs become a problem because of the brittleness of molten explosives. In this case, bending the FLSC may cause cracks to occur inside the explosive. These cracks lead to cut-offs on detonation wave during functioning of FLSC [13].

In this thesis, a new type of molten explosive LSC design is suggested. The liner and the casing are produced according to the profile to be cut. Molten explosive is filled inside of the liner and casing. Then it is cured inside the mechanics.

2.2.3 Plastic Form LSC Production

One way of producing a LSC is using plastic form explosive (for example C-4). Plastic explosive can be assembled into a metallic liner and casing which are produced according to related cut profile [7]. Also, if the liner and the casing are flexible, the design evolve into FLSC since plastic explosive is also flexible, and therefore bending the design to desired profiles is applicable. Explosia and Chemring companies have such products in their datasheets [14, 15], which contain a flexible liner with plastic form explosive. So, it can be bended circumferentially and superficially to cut different profiles. Example of bending of products and view of the targets after the cut are shown in Figure 2-9 and Figure 2-10:

Figure 2-9 Bendability and Functioning of Explosia FLSC [14]

Figure 2-10 Bendability and Functioning of Chemring FLSC [15]

2.2.4 Quality Inspection Methods for LSC

During the production of LSCs, uniformity of density and defects inside the explosive may create some problems. To identify these problems there are 3 different quality inspection methods which are applicable for the products:

- Cutting Method: Two samples are cut from both ends of a LSC. Then these pieces are longitudinally cut and opened to remove the charges inside. These charges are weighed separately. The weight of the charge in each piece divided by the length of that sample gives its linear charge density. Then linear charge densities of both end samples are compared [16].
- Dissolution Method: Two end samples are taken in the same way as in the cutting method. After weighing them, the samples are soaked in acetone to dissolve the charge contained in them. Then they are weighed again after they are dried and cleaned. For each sample, the difference between the two weights divided by the length of the sample gives the linear charge density of that sample. Then linear charge densities of both end samples are compared [16].
- Neutron Radiography (Non-Destructive): It is possible to determine the uniformity of linear charge density distribution. Furthermore, the defects such as sparseness, discontinuity and cavity can also be determined [16].

So, the neutron radiography method is by far advantageous compared to cutting and dissolution methods since it is a non-destructive method. By cutting and dissolution methods it is only possible to measure average density. However linear charge density and defects inside of the explosive for the whole LSC can be determined by neutron radiography.

2.3 Experimental Studies

There are several experimental works [1, 6, 7, 11, 17, 18], which aimed to optimize the penetration efficiency by changing basic parameters like liner type, M/C ratio,

stand-off distance. Among related studies Bohanek, Dobrilovic and Skrlec's approach is more systematic. They assembly plastic form explosive by different amounts of mass on copper and aluminum liners and fire them from different stand-off distances [1]. So, M/C ratio and stand-off distance is optimized for the different liners.

In another work, Burch studies on the effect of firing a LSC under water. He shows that presence of water between the LSC and the target affects the LSC efficiency since water medium is by far denser than air and it slows down the jet velocity and disrupt the formation of jet. So, he suggests by using a foam medium which is less dense than water, the target can be cut more efficiently [19]. Suggested design is given in Figure 2-11.

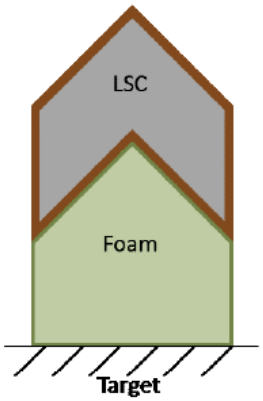

Figure 2-11 LSC Design for Under Water Use [19]

2.4 Simulation Studies

There are several studies which uses AUTODYN and CTH (It is a simulation software code developed by Sandia National Laboratories which is designed to treat material motion and shock wave propagation in 1D, 2D and 3D. In the literature, it is rarely used compared to AUTODYN.) programs to simulate jet formation and penetration of LSC [4, 5, 6, 17, 20, 21, 22]. Differing from other studies, Johnston and Lim simulate a LSC in 3D and find meaningful penetration results with

experiments [21]. Considering the long duration of explicit simulations, 3D approach is rarely used for LSC jet formation and propagation. LSC model before and during the initiation are given in Figure 2-12. Comparison of the 3-D simulation and experimental results of a LSC is shown in Figure 2-13:

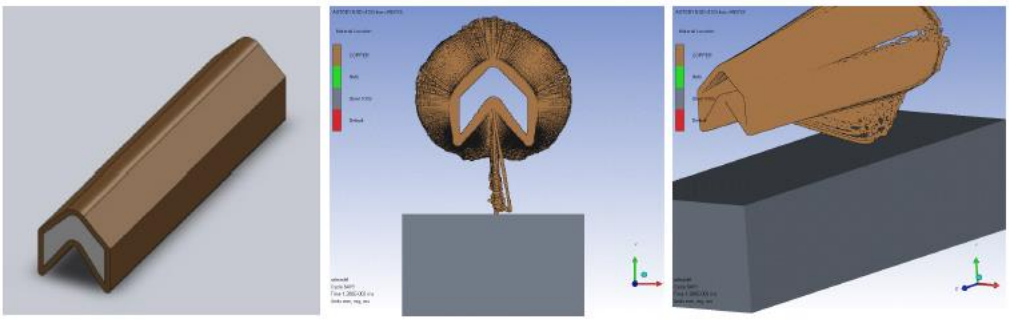

Figure 2-12 3D LSC Simulation Before and During the Initiation [21]

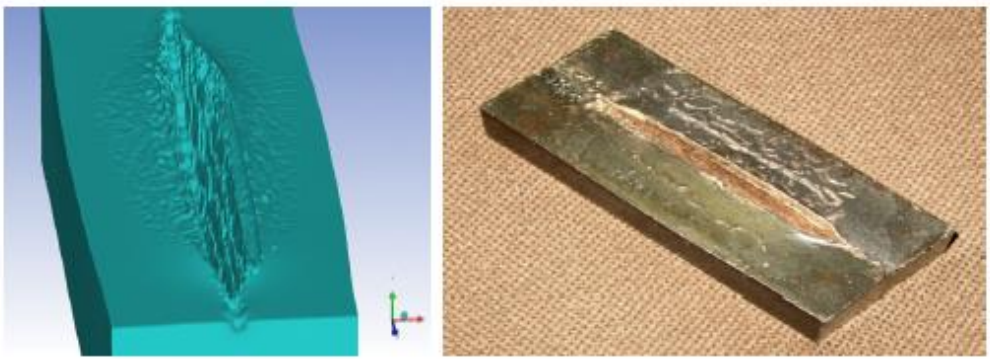

Figure 2-13 3D LSC Simulation, Target Material Comparison with Experiments After the Penetration [21]

In the literature, there are also some useful simulation studies for Shaped Charges and they can be adapted to LSCs by changing symmetry axis from axial to planar. One of them is Gürel's work in which the shaped charge jet formation and penetration problems are treated separately by using AUTODYN. First, he models the jet formation on Euler space, then simulate the penetration on Lagrange space by transforming the Euler jet to Lagrange by using part filling option of the AUTODYN. Then, he gets consistent penetration results with experiments [23].

Furthermore, decreasing detrimental effects of LSCs on its environment can be another challenge especially for the rocket systems which is important to protect the systems close to functioning LSC. Bingöl has investigated these effects with experiments and AUTODYN simulations. By positioning backspace plates with varying distances, he examined the buckling damage on the plates and matched the experimental results with the simulations [24]. Bingöl's test set-up is given in Figure 2-14:

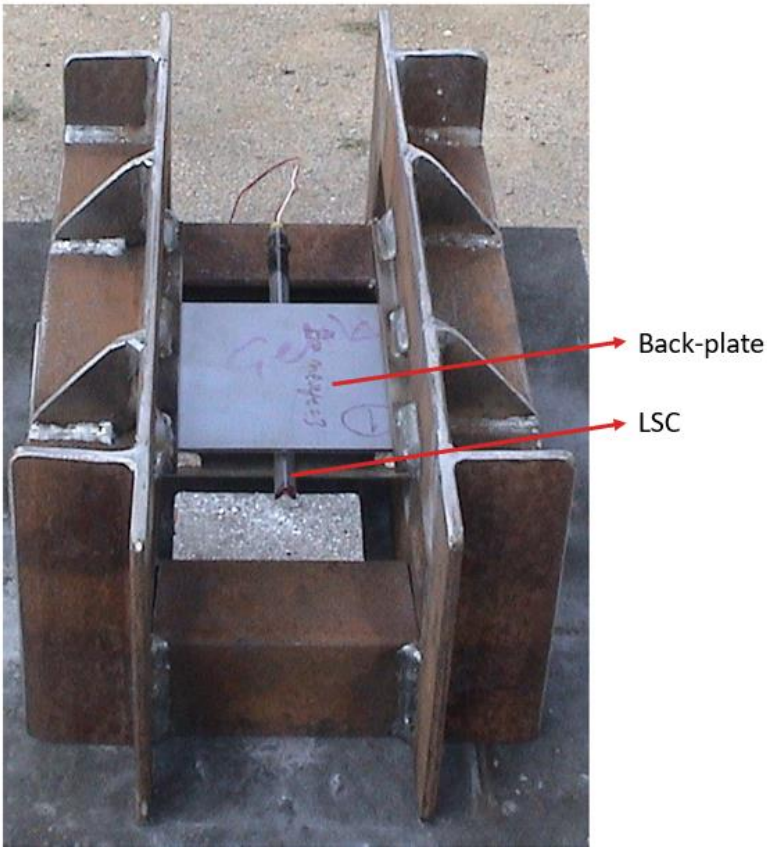

Figure 2-14 LSC Test Set-up to Determine the Detrimental Effects of a LSC on a Back-plate [24]

The numerical and experimental comparison of the damage created on the back-plate for different specimens is provided in Figure 2-15:

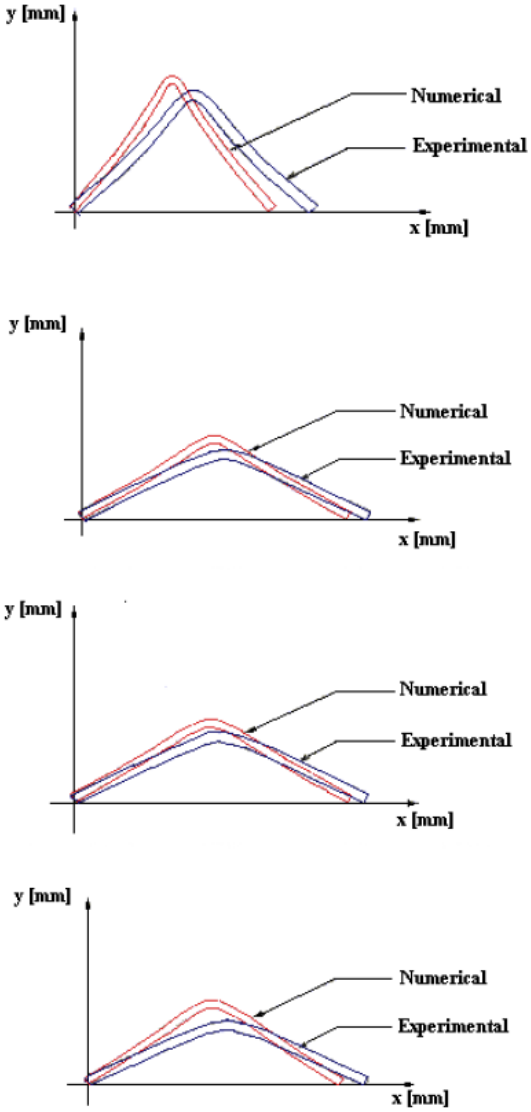

Figure 2-15 Numerical and Experimental Comparison of the LSC on the Back-plate for Different Specimens [24]

2.5 Analytical Studies

LSC jet formation and penetration problems can also be solved by using theoretical formulas. In the literature, the common procedure is to divide the design parts into small elements and to apply related formulas. Gürel applies those formulas into jet formation and penetration of a SC and compares the results with simulations and experiments. He also compares the results of analytical formula alternatives and

shows which ones fit better with the simulation and experiment results [23]. Theory of the jet formation, jet penetration and jet break-up are reviewed in detail in Sections 4.1, 4.2 and 4.3 respectively.

CHAPTER 3

CIRCULAR LINEAR SHAPED CHARGE EXPERIMENTS

3.1 CLSC Prototype Productions

3 different prototype configurations are designed for the targets having different cutting region geometries. In the first design a LSC configuration is produced for straight line cutting. In the second one, a CLSC design is produced which can be used to cut circular plane targets. In the last configuration, a CLSC design is produced to cut tube targets from inside of them.

3.1.1 LSC Configuration

Linear copper liner cross-sectional dimensions and isometric view which is produced for LSC production are shared in Figure 3-1. ETP (Electrolytic-tough Pitch Copper) type copper is selected for its easy availability and high dynamic yield strength which is advantageous for higher break-up times [23]. OFHC (Oxygen-free Copper) type copper dynamic yield strength is higher than ETP type copper [23], but it is not selected since OFHC is less available in the market. Then, a plastic bonded explosive (%88 HMX, %12 plastic) with a 5.4 mm thickness were assembled onto copper liner. Final form of the configuration is given in Figure 3-2.

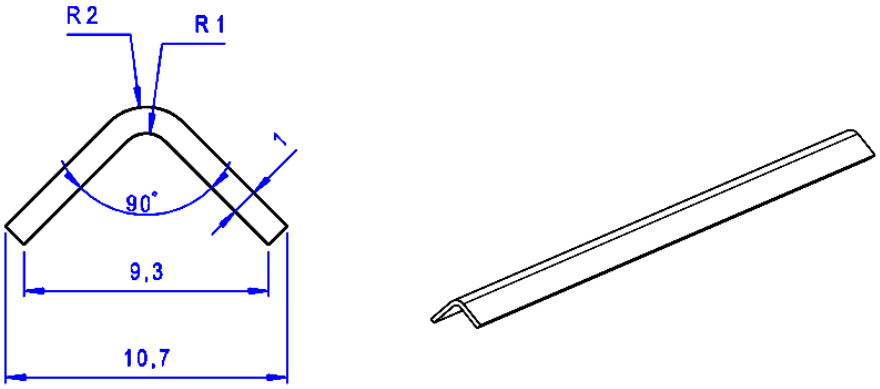

Figure 3-1 LSC Cross-sectional Dimensions and Isometric View

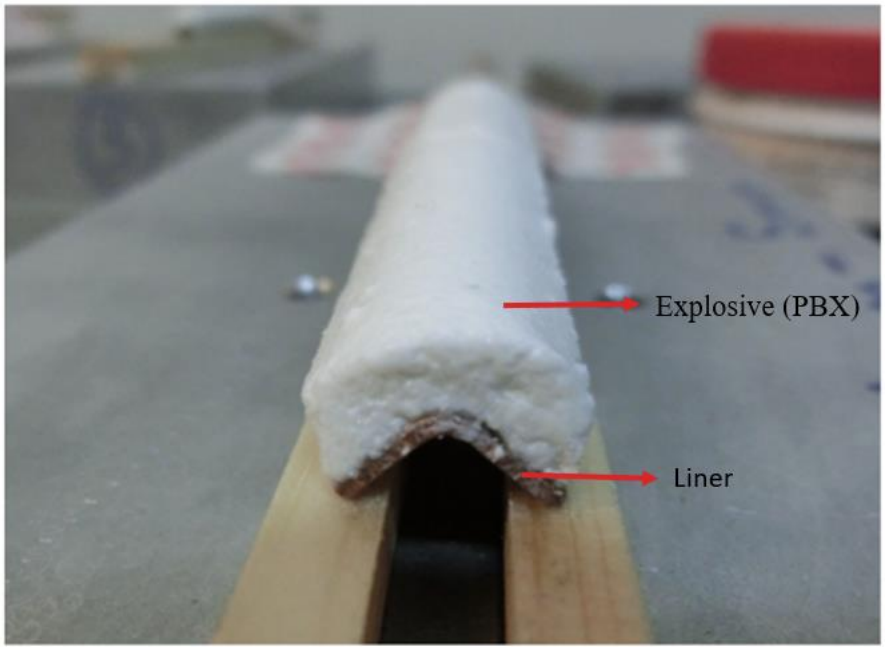

Figure 3-2 LSC prototype

3.1.2 CLSC (On Plane) Configuration

A Circular Linear Shaped Charge is designed to cut on plane targets circularly. Firstly, an aluminum housing and copper liner was produced by machining operation. For the aluminum housing 6061-T6 type material is selected because of its higher strength value than average and easy availability in the market. ETP type

copper is selected again for its easy availability and high dynamic yield strength. Isometric view, cross-sectional view and the related dimensions of the mechanics are given in Figure 3-3.

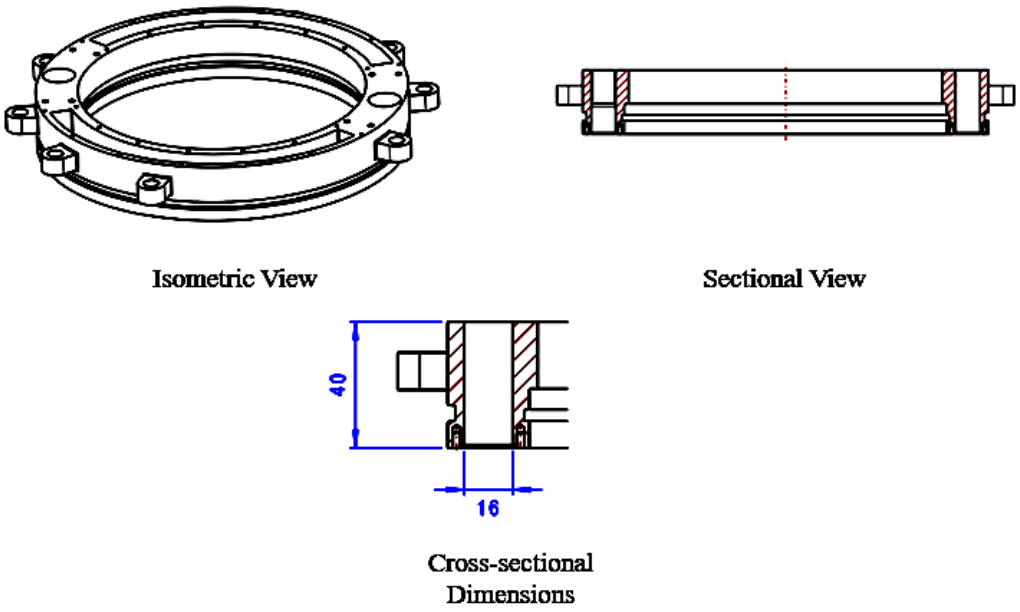

Figure 3-3 CLSC (On Plane), Aluminum Housing Isometric View, Cross-sectional View, and Related Dimensions

After the production of the mechanics, housing and the liner assembled with 8xM3 cylinder head bolts. Then, PBX-110 molten explosive was poured down from the upper side of the housing with four different masses which are 200, 225, 250 and 325 grams. The explosive assembly was vibrated for 30 minutes to homogenize the explosive level inside the housing, then was cured at 60 °C for 1 week to solidify the molten explosive. The isometric view of CLSC (On Plane) from top and bottom are given in Figure 3-4 and Figure 3-5. Cross-sectional view of CLSC (On Plane) is shared in Figure 3-6.

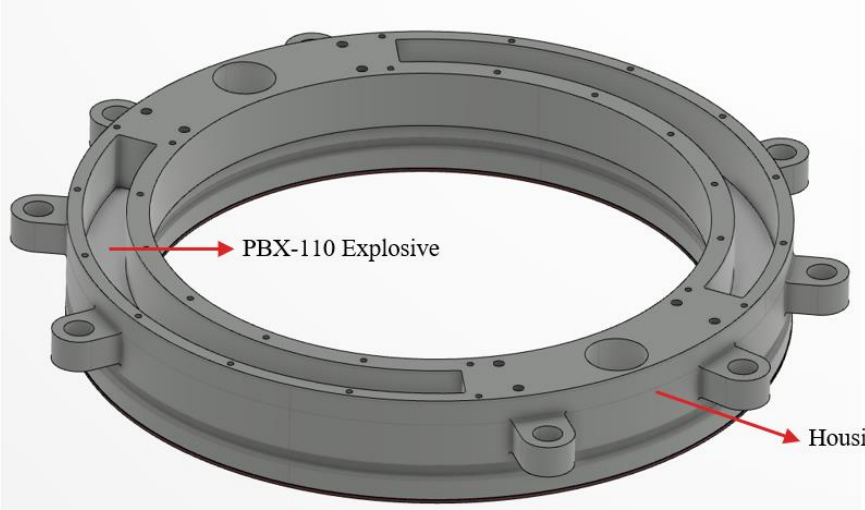

Figure 3-4 Isometric View (From Top) of CLSC (On Plane)

Figure 3-5 Isometric View (From Bottom) of CLSC (On Plane)

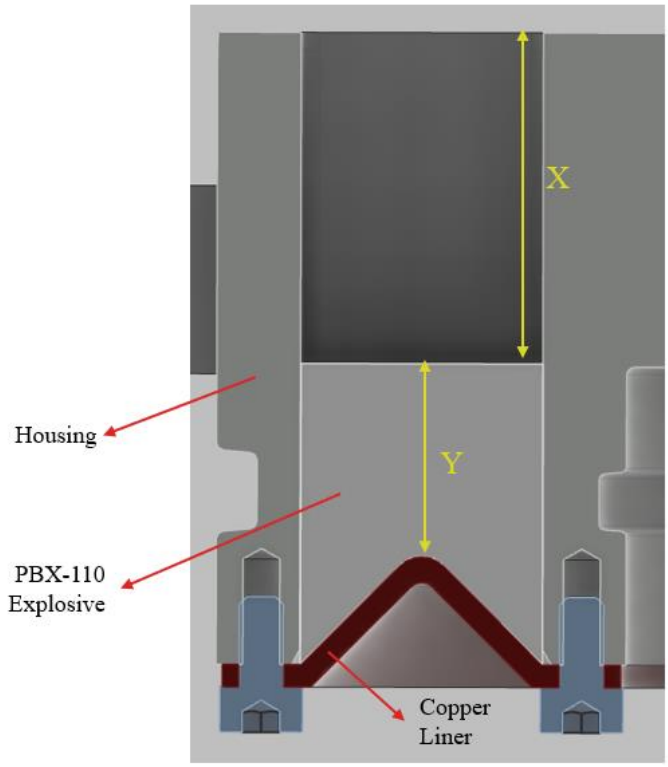

Figure 3-6 Cross-sectional View of CLSC (On Plane)

Total 4 prototype was produced for each explosive mass. The distance from explosive surface to upper surface of housing (Dimension X, see Figure 3-6) for each prototype with their variance and the explosive length from the apex of the liner (Dimension Y, see Figure 3-6) are given at Table 3-1. Related dimensions were determined by measuring it from 16 different equally spaced distance by caliper for each of the prototypes.

Table 3-1 CLSC (On Plane) Prototype Production Data

Prototype #	**Explosive Mass (grams)**	**Dimension X (mm)**	**Variance of X (mm)**	**Dimension Y (mm)**
1	200	21.3	±0.2	6.4
2		21.1	±0.25	6.65
3		21.0	±0.45	6.75
4		21.1	±0.4	6.6
5	225	20.1	±0.6	7.6
6		19.9	±0.45	7.85
7		20.0	±0.55	7.75
8		20.0	±0.3	7.7
9	250	18.7	±0.3	9
10		18.9	±0.45	8.85
11		18.9	±0.75	8.85
12		18.7	±0.4	9
13	325	14.2	±0.7	13.5
14		13.5	±0.5	14.2
15		15.1	±0.15	12.65
16		14.9	±0.7	12.8

3.1.3 CLSC (On Tube of Inner Radius) Configuration

As a separate work, a Circular Linear Shaped Charge is designed to cut tube shaped targets from inner radius of it. An aluminum housing and a copper liner were produced by machining operation similar to the on plane CLSC design. Again 6061-T6 aluminum and ETP copper materials were selected for the housing and the liner. After the production of the mechanics, the housing and the liner were assembled with 48xM3 cylinder head bolts. Then, 450 grams PBX-110 molten explosive was poured down from the upper side of the housing of two prototypes. The explosive assembly was vibrated for 30 minutes to homogenize the explosive level inside the housing, then was cured at 60 °C for 1 week as in the CLCS (On Plane) productions. Isometric view of the CLSC (On Tube of Inner Radius) is shared in Figure 3-7. Related cross-sectional dimensions of the CLSC are shared in Figure 3-8.

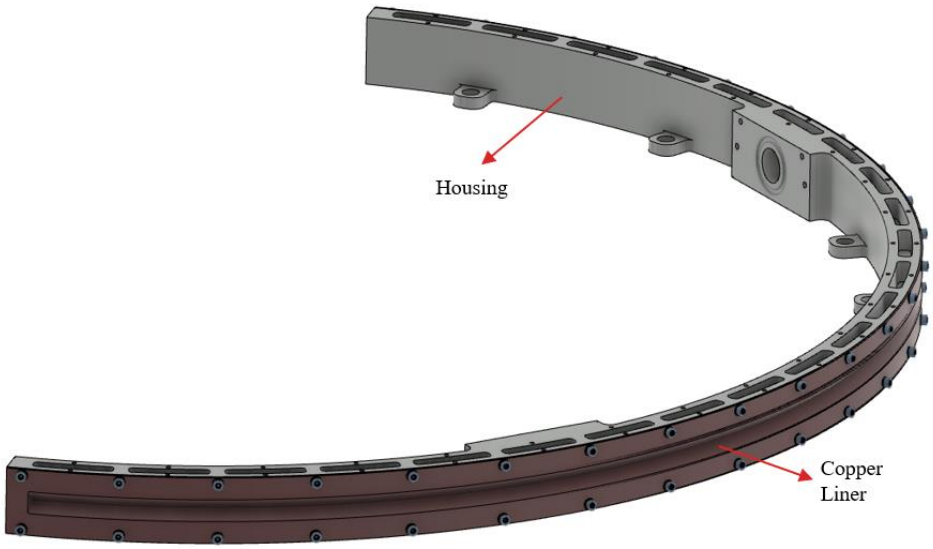

Figure 3-7 CLSC (On Tube of Inner Radius) Isometric View

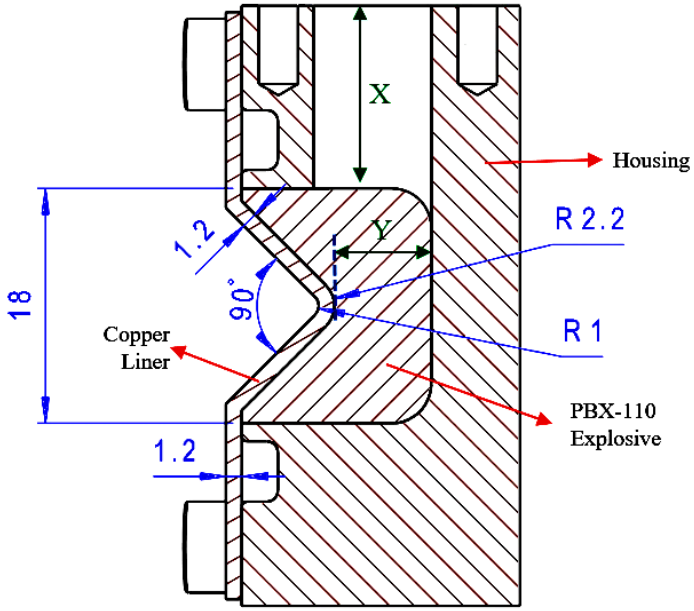

Figure 3-8 CLSC (On Tube of Inner Radius) Cros-sectional and Related Dimensions

The distance from explosive surface to upper surface of housing (Dimension X, see Figure 3-8) for each prototype with their variance and the explosive height from the apex of the liner (Dimension Y, see Figure 3-8) are given at Table 3-2. Related dimensions were determined by measuring it from 20 different equally spaced distance by caliper.

Table 3-2 CLSC (On Tube of Inner Radius) Prototype Production Data

Prototype #	**Explosive Mass (grams)**	**Dimension X (mm)**	**Variance of X (mm)**	**Dimension Y (mm)**
1	450	13.6	±0.4	7.2
2		13.4	±0.5	7.2

3.2 CLSC Firing Tests

3.2.1 LSC Tests

2 LSC prototypes were fired with Teledyne RP-80 EBW detonators (containing 0.1 grams high explosive) on 7075-T6 aluminum targets from 10 mm and 15 mm stand-off distances. The detonator was enclosed with an aluminum part to direct the detonation on the main charge of the LSC. Stand-off distance of the prototypes were adjusted by 10 mm and 15 mm wooden blocks which were assembled between the LSC and the target. Test set-up is given in Figure 3-9.

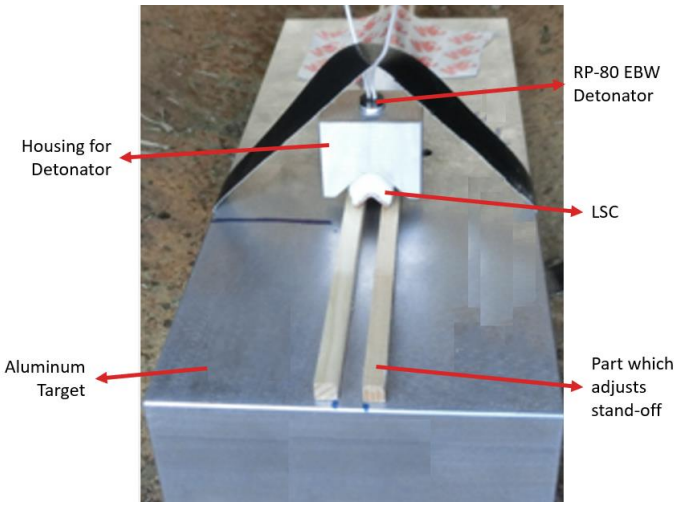

Figure 3-9 LSC Test Set-up

The minimum, average, and maximum penetration results are given at Table 3-3. The penetration depths were measured at 2 mm equidistant points by caliper. According to results, prototypes are penetrated averagely 10.9 and 13.3 mm for 10 and 15 mm stand-off distances, respectively. For prototype #1, the results show that the jet velocity cannot reach its maximum so there is need for more stand-off distance to have a larger penetration. Since the penetration for prototype #2 is larger, it can be concluded that the jet velocity forms more effectively than prototype #1.

Table 3-3 LSC Test Penetration Results

Prototype #	(M/C)* Ratio	Stand-off Distance (mm)	Minimum Penetration (mm)	Average Penetration (mm)	Maximum Penetration (mm)
1	0.8	10	8.7	10.9	12.5
2		15	10.5	13.3	15.4

** M/C: (Liner/Explosive Mass Ratio)*

Penetration on the aluminum target from top view and cross-sectional view are shown in Figure 3-10 and Figure 3-11. In Figure 3-11, it can be seen that the penetration is lower at the initiation region of the LSC compared to other parts.

Figure 3-10 LSC, Target Top View after the Penetration

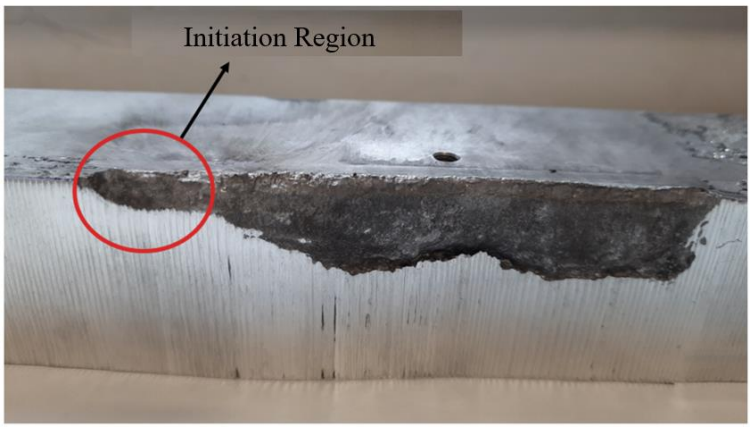

Figure 3-11 LSC, Target Section View after the Penetration

3.2.2 CLSC (On Plane) Tests

CLSC (On Plane) prototypes were fired with Teledyne RP-83 EBW detonators (containing 1 grams high explosive) on 20 mm thick, 4140 steel (32-36 HRC) targets at 17 mm and 22 mm stand-off distances. Steel target thickness was selected thicker than expected penetration depths intentionally to examine the penetration performance at different explosive mass and stand-off values. Test set-up is given in Figure 3-12.

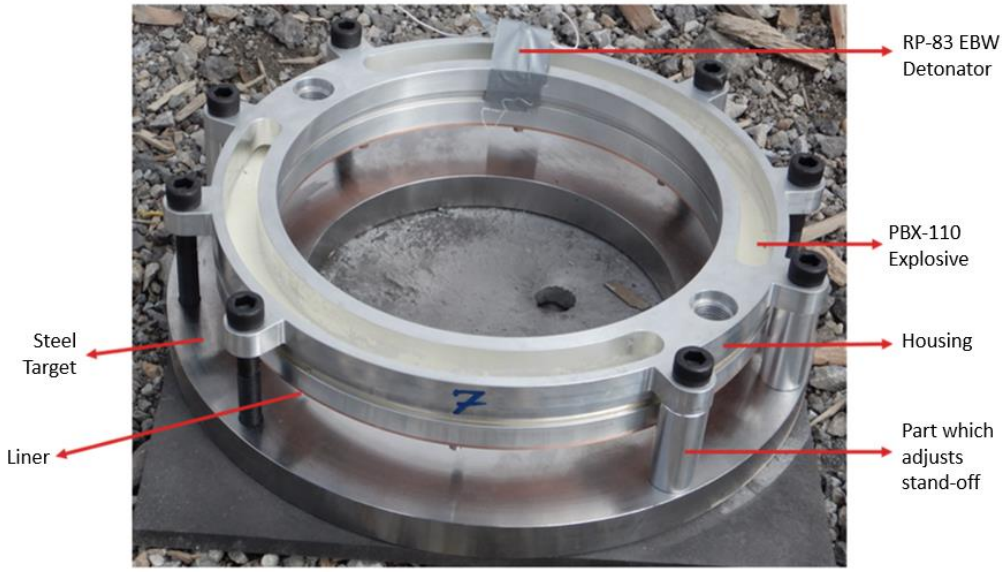

Figure 3-12 CLSC (On Plane) Test Set-up

The minimum, average, and maximum penetration results are given at Table 3-4. The penetration depths were measured at 24 equiangular points by caliper.

Table 3-4 CLSC (On plane) Test Penetration Results

Prototype #	M/C Ratio	Stand-off Distance (mm)	Minimum Penetration (mm)	Average Penetration (mm)	Maximum Penetration (mm)
1	1.06	17	7.5	8.75	9.5
2			7.5	9.0	10.0
3		22	7.0	9.2	11.0
4			6.4	8.5	9.8
5	0.94	17	8.8	9.5	11.1
6			8.5	9.3	11.0
7		22	8.4	9.4	10.2
8			9.5	10.1	11.5
9	0.84	17	9.4	10.5	11.7
10			9.3	10.8	12.7
11		22	9.0	10.5	12.0
12			10.2	11.0	12.7
13	0.65	17	10.3	11.6	13.0
14			12.2	13.5	15.0
15		22	13.0	14.9	16.7
16			11.0	12.5	14.0

Relation between the average penetration and M/C ratio for 17 mm and 22 mm stand-off is given in Figure 3-13. As seen in Figure 3-13, as the M/C ratio decreases the average penetration increases irrespective of the stand-off distances considered. Since the rate of increase in penetration does not decrease as M/C ratio decreases from 1.06 down to 0.65, it can be concluded that the jet velocity does not reach its saturation value at M/C=0.65. Therefore, decreasing the M/C ratio (in other words by increasing the explosive mass) below 0.65 may result higher penetration values for both standoff distances.

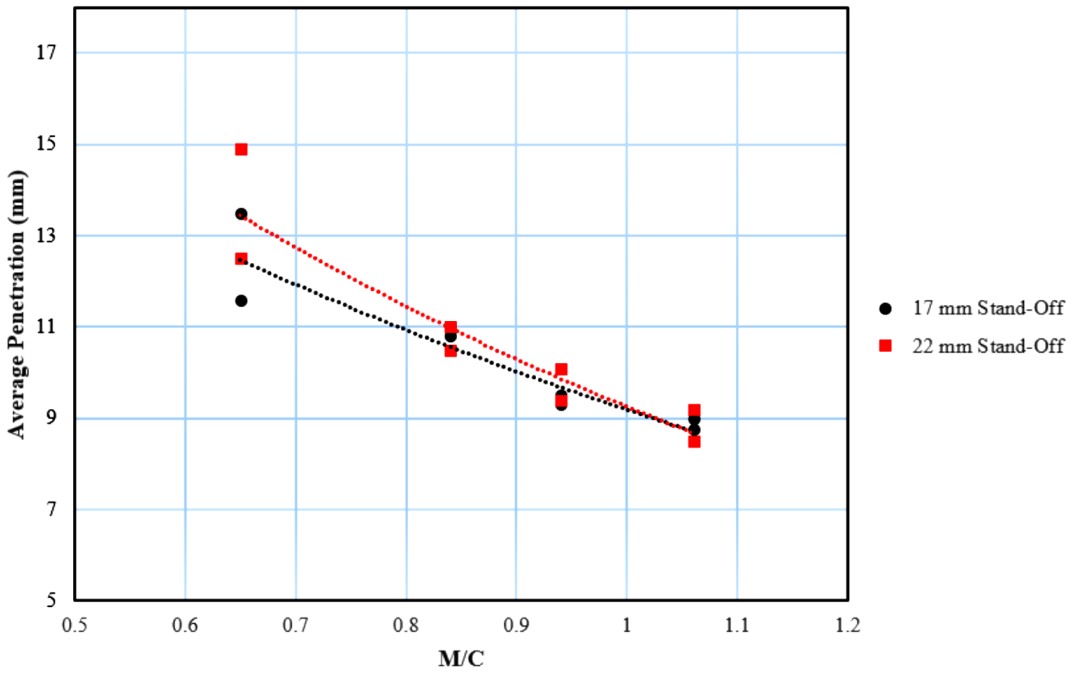

Figure 3-13 CLSC (On-Plane) M/C vs. Average Penetration (mm) Plot

Penetration on the steel target from top view and cross-sectional view are given in Figure 3-14 and Figure 3-15.

Figure 3-14 CLSC (On Plane) Penetration on Target (Top View)

Figure 3-15 CLSC (On Plane) Penetration on Target (Cross-sectional View)

3.2.3 CLSC (On Tube of Inner Radius) Tests

A tube-shaped target which has 4 different tube thicknesses on the same part was produced from 7075-T6 aluminum. In each 90° angle of the tube, there is a different tube thickness. These 4 different tube thicknesses are 19 mm, 22 mm, 25 mm, and 28 mm. The outer diameter of the tube is kept constant, so changing the tube thickness also changes the stand-off distance of the CLSC. Then the stand-off distances have formed as 21 mm, 18 mm, 15 mm, and 12 mm respectively. Different thicknesses of the part and the formation of different stand-offs are given in Figure 3-16.

2 CLSC (On Tube of Inner Radius) prototypes were fired with Teledyne RP-83 EBW detonators. One prototype was assembled to tube in the position to cut 19 mm and 22 mm thickness surface while the other prototype was assembled to cut 25 mm and 28 mm thickness. Test set-up is given in Figure 3-17.

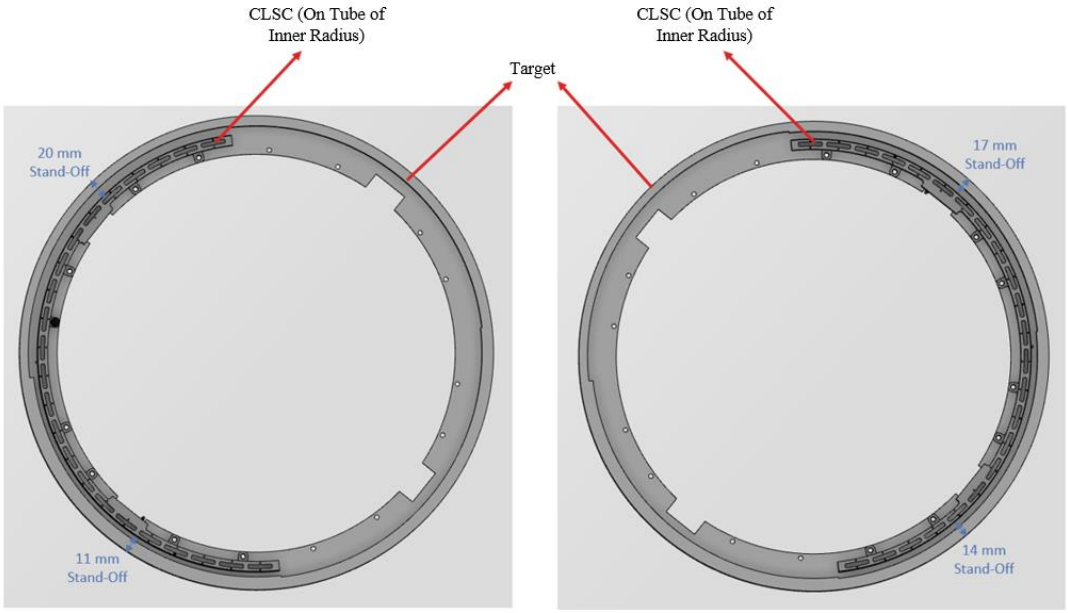

Figure 3-16 CLSC (On Tube of Inner Radius) Set-up Top View

Figure 3-17 CLSC (On Tube of Inner Radius) Test Set-up

In both firings, CLSC prototypes cut the targets completely although the aim was the comparison of the effect of the different stand-off distances to penetration. Complete penetration of the jet from the broken piece of target tube is given in Figure 3-18,

part (a). To clarify the related figure, cross-sectional view of the tube before and after jet penetration are shown in Figure 3-18, part (b) and part (c), respectively.

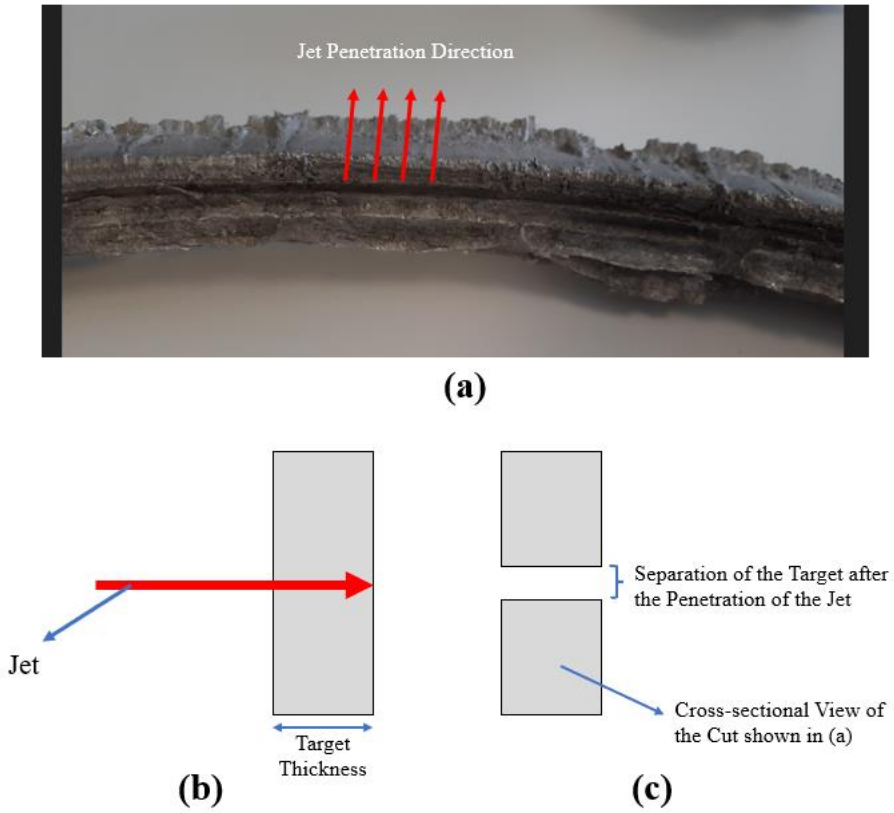

Figure 3-18 CLSC (On Tube of Inner Radius) Target Tube Examination after the Penetration

CHAPTER 4

ANALYTICAL MODELLING OF CIRCULAR LINEAR SHAPED CHARGE AND COMPARISON WITH EXPERIMENTS

In the literature, there are lots of analytical 1D models for the Shaped Charges (SC) which are used for jet formation and penetration on the target. These models are very practical because they offer faster solutions comparing with explicit simulations. Also, checking the simulation results with the analytical models can help to ensure accuracy of the designs.

Theoretical formulas which are used for SCs can also be applied for LSC modelling since the jet formation and the penetration procedures are the same at 1D for the SC and LSC. During the modelling, the main difference between SC and LSC is the formulation of the liner to explosive mass ratio μ from apex axis to base of the liner because of the difference of the geometries. Accurate models can be formed for LSCs by the same SC theoretical formulas by being aware of this difference.

4.1 Jet Formation Modelling

Baker defines the jet formation for a SC by 4 separate processes which are detonation of explosive, liner collapse, point jetting collapse , and jet stretching, respectively [25]. These processes are given below, they can also be followed visually from the Figure 4-1.

a) Detonation of Explosive: When the main charge of the SC is detonated by an initiator, detonation propagates with a velocity D. As the detonation wave reaches to liner, it transforms to tangential sweep velocity U_{det} which is the multiplication of the D with cosines of angle of incidence γ.

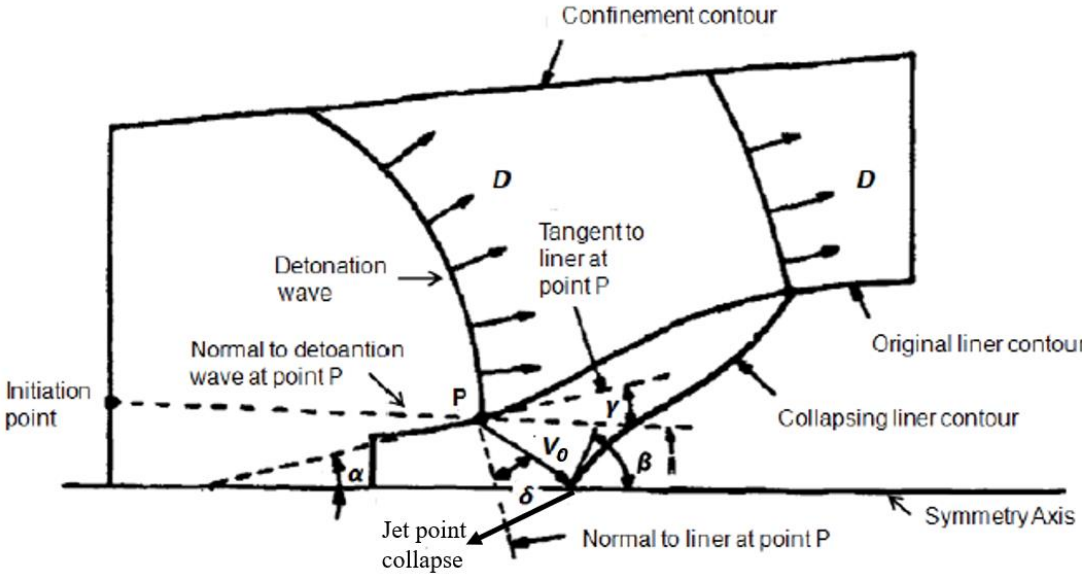

Figure 4-1 Collapse of a Shaped Charge Geometry [23]

b) Liner Collapse: As the detonation wave interacts with the SC liner, liner elements are accelerated due to high pressure possessed in the explosive. Then, the liner elements start to move on towards to symmetry axis of the SC with projection angle δ and an accelerating collapse velocity V_0.

c) Point Jetting Collapse: Accelerated liner elements meet on the symmetry axis and forms a one-dimensional jet liner. Position of the elements where they gathered is named as collapse point. It's an active position and it moves forward instantaneously with a velocity V_c on the symmetry axis. The elements which is gathered at the symmetry axis may move on forward or backward according to design of SC which they called jet velocity V_j and slug velocity V_s (portion of the jet which does not contribute to penetration due to low velocity), respectively.

d) Jet Stretching: For the most part of the jet, jet elements stretch because of the positive velocity gradient. Unlike the other regions, typically a negative velocity gradient occurs on the tip of the jet which causes a mass accumulation in front of it. But cumulatively, jet stretches due to the average positive velocity gradient.

As a result, Baker's jet formation definition for the SC is also valid for a LSC. Furthermore, the Figure 4-1 can also be simplified for LSC since the position of the initiation axis is on the symmetry axis and the angle of incidence γ is equal to apex angle α due to "V" shape of the liner.

In the next items, related formulas are introduced which is used for the formation of jet in LSC modelling. In some of the items, there are also different formula names which can replaced with them but they are not shared explicitly, yet their names and resources are available inside of it.

4.1.1 Collapse and Acceleration of the Liner

Trinks [mentioned in 26] derived the following formula for the initial collapse velocity:

$$V_0 = 0.36D \tan^{-1}\left(\frac{2}{3}\mu\right) \qquad (1.1)$$

Where; D: detonation velocity, μ: liner to mass ratio.

Chou-Flis , Duvall , Mikhailov and Dremin and Shushko have also derived formulas to calculate initial collapse velocity [mentioned in 26]. These terminal collapse velocity formulas are derived by empirical relationships which are corporated with a final velocity model.

Calculating initial collapse velocity of the liner elements is not enough since the elements has an acceleration while moving to symmetry axis. To take the acceleration into account, Randers-Pehrson has derived the following formula [mentioned in 26]:

$$V(t) = V_0\,[1\text{-}\exp(-(t\text{-}t_0)/\tau)] \qquad (1.2)$$

Where; t: current time, t_0: initial time, τ: time constant.

Chou suggests the following formula to derive τ, which is based on initial momentum considerations:

$$\tau = (C_1 MV_0/P_{cj}) + C_2 \qquad (1.3)$$

Where; P_{cj}: Chapman Jouget pressure, C_1 & C_2: Explosive parameters which can be determined empirically from experiments.

4.1.2 Collapse of Liner

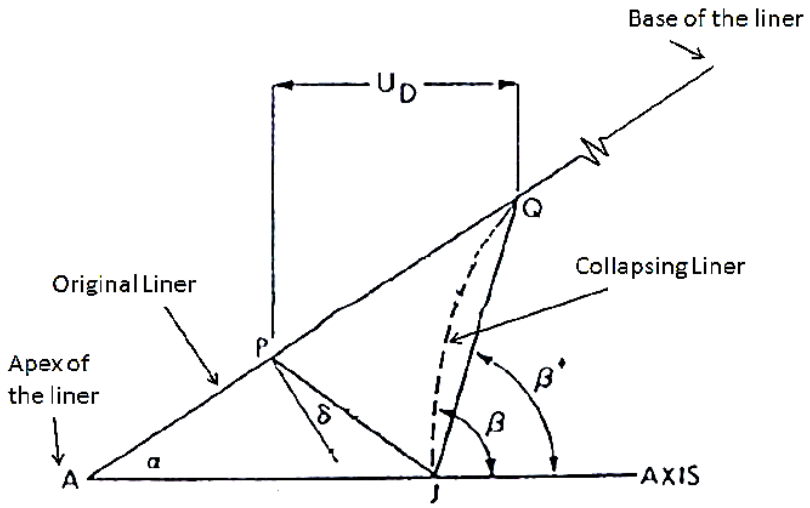

Figure 4-2 Sketch of Liner Collapse [26]

Liner collapse process is explained clearly in Güler's study [23]. Figure 4-2 can be followed while examining these explanations:

During the collapse process of a liner element (for example the element is at the point P before it starts to move, then it reaches to point J in Figure 4-2), it makes an angle of δ with the normal of the liner surface. This angle is related with V_0 and U_{det} by Taylor [27] in the following formula:

$$sin\,\delta = V_0/2U_{det} \qquad (1.4)$$

Where; V_0: Initial collapse velocity, U_{det}: Sweep velocity.

Collapse of the liner is a transient process since it has acceleration, but firstly it is needed to calculate the collapse angle as if it is in steady state. Steady state collapse angle β^+ can be defined as in the following formula [mentioned in 26]:

$$\beta^{+} = \alpha + 2\delta \qquad (1.5)$$

In real case, the collapse velocity decreases from apex to base with a non-conical contour of a collapsing surface (see Figure 4-2). So the collapse angle can not be directly calculated by Equation 1.5. Then, by using calculated steady state collapse angle β^{+}, the corrected collapse angle β can be calculated by the following formula:

$$\tan\beta = \frac{\left(\sin\beta^{+} - X\ \sin\alpha(1 - \tan(A)\tan(\delta))\frac{V'_0}{V_0}\right)}{\left(\cos\beta^{+} + X\ \sin\alpha(\tan(A) + \tan(\delta))\frac{V'_0}{V_0}\right)} \qquad (1.6)$$

$$\text{where } A = \frac{\beta^{+} + \alpha}{2}$$

Where; V'_0: Derivative of the collapse angle with respect to liner height, X: Position of the liner element on X axis

In the related formula, V'_0 is derived by considering the effect of changing collapse velocity (V_0) which is the derivative of the collapse angle (β) with respect to liner element position. Also, variable-A (deflection angle) is defined as the angle that a liner element moves to the symmetry axis.

4.1.3 Jet and Slug Velocity Calculations

Jet velocity V_j and slug velocity V_s of a collapsed liner element is formulated by Pugh, Eichelberger and Rosteker which is known as P-E-R theory [28]. They formulated V_j and V_s by using initial collapse velocity V_0, apex angle α, projection angle δ and corrected collapse angle β. In the calculation of V_j and V_s, final collapse velocities of liner elements depend on the original positions on the liner. So, projection angle δ and corrected collapse angle β change according to the position of the elements. The related formulas are given below:

$$V_j = \frac{V_0 \cos(\alpha + \delta - \frac{\beta}{2})}{\sin(\frac{\beta}{2})} \qquad (1.7.a)$$

$$V_s = \frac{V_0 \cos(\alpha + \delta - \frac{\beta}{2})}{\cos(\frac{\beta}{2})} \qquad (1.7.b)$$

4.1.4 Jet Tip Formation

For SC or LSC, formation of the jet is about positive velocity gradient from apex to base of the liner. Yet, the distance from liner to symmetry axis near the apex is very small, so the elements near the apex cannot be accelerated and therefore a mass accumulation happens on the tip of jet [mentioned in 23]. Then, the jet tip velocity should be modified by considering this effect. Modified jet tip velocity formula is given below [mentioned in 23]:

$$V_{tip} = \frac{\int_0^{m_{tip}} V_j \, dm_j}{\int_0^{m_{tip}} dm_j} \qquad (1.8)$$

Where; m_j: Mass of the element V_j: Velocity of the element.

4.2 Jet Break-up Modelling

It is important to model the jet break-up while calculating the jet penetration on the targets. If the jet break-up begins, jet particles start to tumble and disperse from the symmetry axis and these leads decrease in the penetration efficiency of the jet.

There are several semi-empirical formulas in the literature which models the jet break-up time of the jet elements (for example Hirch model [29], Pfeffer model [29], Chou-Carleone model [26], Chou model [29]). They are derived from flash X-Ray experiments by the observation of the break-up time of different SC configurations. In this study, Hennequin's break-up model is used [29]. Hennequin developed this model for SCs but it can also be used for LSC. The first step is calculating the plastic velocity V_{pl} . It can be defined as the velocity propagation of plastic instabilities on the jet. It can also be visualized as the average velocity difference between successive jet particles after the break-up of the jet.

$$V_{\text{pl}} = \sqrt{\frac{Y}{\rho_{\text{liner}}}} \qquad (1.9)$$

Where; Y: Dynamic yield strength of the liner, ρ_{liner}: Density of the liner.

Dynamic yield strength of some common liner materials is gathered by Güler at Table 4-1 [23].

Table 4-1 Dynamic Yield Strength of Some Common Liner Materials

Liner Material	**Y, Jet Yield Strength (GPa)**
Copper ETP	0.2
Copper OFHC	0.27
Aluminum	0.1

Then, the break-up time of the liner can be calculated by the following semi-empirical formula for each element:

$$t_b = 2.92\ (r/V_{pl}) + 0.46\ (L/\ V_{pl}) \qquad (1.10)$$

Where; r: Initial radius of jet element L: Length of the jet (from AUTODYN simulations).

"r" can be calculated by equating the volume of liner element to jet element which forms on the symmetry axis of the apex.

4.3 Jet Penetration Modelling

1D jet penetration modelling is based on the Bernoulli principle and its modifications related to empirical observations.

According to Birkhoff's hydrodynamic penetration theory, penetration velocity of the jet element can be predicted by applying Bernoulli equation [30]. As a jet element which has a jet velocity V, penetrates a target, a stationary penetration velocity U occurs which can be derived from following equation:

$$\frac{1}{2}\,\rho_j\,(V-U)^2 = \frac{1}{2}\,\rho_t\,(U)^2 \qquad (1.11)$$

Where; ρ_j: Density of the jet, ρ_t: Density of the target.

All the jet/target interactions have a cut off velocity which the penetration cannot occur below this value. So, calculating the penetration velocity U is important while computing the penetration on the target.

Classical penetration theory accounts only the jet and target density while calculating the penetration velocity U, but it is known that the material strength is also an important property for U. Tate and Alekseevski proposed the following formula by adding target resistance R_t and penetrator resistance Y_p terms into hydrodynamic theory [31]:

$$\frac{1}{2}\,\rho_t\,(U)^2 + R_t = \frac{1}{2}\,\rho_p\,(V-U)^2 + Y_p \qquad (1.12)$$

There are suggested values for R_t and Y_p. Table 4-2 shows the suggested values for R_t and Y_p. However, correlating these constants to match with the penetration results of experiments is evaluated as a better method to determine the R_t and Y_p [mentioned in 23].

Table 4-2 Suggested R_t and Y_p Values for Common Liner and Target Materials

Material	**Suggested Value for R_t and Y_p**
RHA	4.5 times yield stress of the material
Steel	5-6 times yield stress of the material
Aluminum	4-5 times yield stress of the material

First the penetration velocity U is calculated. If U is higher than the cut-off velocity, the penetration of the liner element can be found by using the following formula:

$$P = l\sqrt{\frac{\rho_j}{\rho_t}} \qquad (1.13)$$

Where; ρ_j: Density of the jet, ρ_t: Density of the target, l: length of the jet element.

Suggested penetration formula only takes into account the jet and target densities but again strength of the materials is also important as in the penetration velocity calculations. So, Pack and Evans developed the following semi-empirical formula by adding yield strength of the target Y, experimental constant α and, element jet velocity terms V [32]:

$$P = l\sqrt{\frac{\rho_j}{\rho_t}}\left(1 - \frac{\alpha\, Y}{\rho_j V^2}\right) \qquad (1.14)$$

According to Pack-Evans formula, the effect of the target yield strength Y increases as the penetration velocity decreases. So, it can be deducible from the related formula that the hydrodynamic assumptions are less effective especially for the lower penetration velocities.

4.4 Analytical Code Methodology

LSC/CLSC jet formation and penetration analytical code has written in MATLAB program. The code has two stages, the first one is the formation of the jet and the second one is the penetration.

At the formation of jet stage, the liner is divided into predefined "n" number of elements equidistant from each other. Before starting the code, design parameters (the apex angle, liner width, liner thickness, liner to explosive mass ratio μ, stand-off distance) should be entered. Then, according to theory of Section 4.1, elements start to collapse into symmetry axis. When an element reaches to symmetry axis, jet velocity V_j is calculated for the element. Then, the element begins to move onto target, and their positions are found after each a predefined time step t_s. The movements of all elements continue until one of the jet elements reaches out to target surface. Modelled LSC/CLSC for the analytical code is given in Figure 4-3. Jet formation calculation can be followed from the flow chart in Figure 4-4.

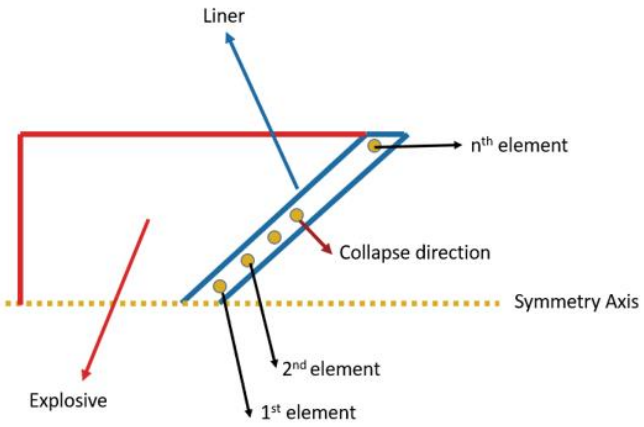

Figure 4-3 LSC/CLSC Modelling for the Analytical Code

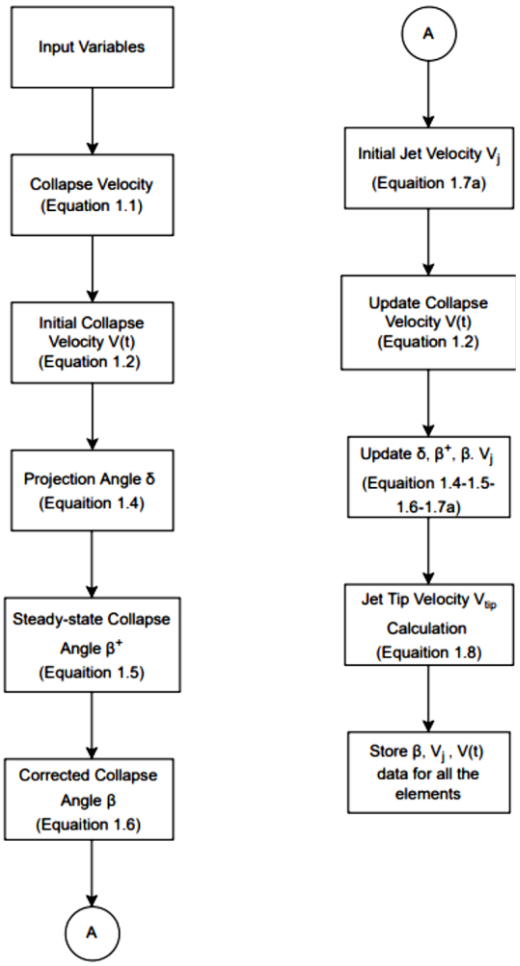

Figure 4-4 Flow Chart of Analytical Code for Jet Formation

As one of the jet elements reach out to the target surface, the related element creates a penetration line ℓ between an element which is the closest to it (Figure 4-5). Then, the penetration of the line is calculated according to Tate-Alekseevski and Pack-Evans formulas which is discussed in Section 4.3.

$$P = l\sqrt{\frac{\rho_j}{\rho_t}}\left(1 - \frac{\alpha Y}{\rho_j V^2}\right)$$

Figure 4-5 Penetration Line and Application of it to Pack-Evans Formula

After the calculation, penetration value is stored in the code, and the element is deleted. Target surface position is updated as much as the penetration value (For example if the target surface begins at 10 mm at the symmetry axis and the element penetration is 1 mm, then the new target surface position becomes at 11 mm, and the new element should reach at 11 mm position to keep up the penetration). The code continues with the elements which are not penetrated to target until all the elements deleted from the code. Then, the total penetration is equal to the summation of the penetrations of the jet elements. Sketch of the jet elements movement through the target and their penetration are shown in Figure 4-6. Penetration of the jet can also be followed from the flow chart in Figure 4-7.

Figure 4-6 Sketches of Jet Element Movement (a) and Penetration to Target (b)

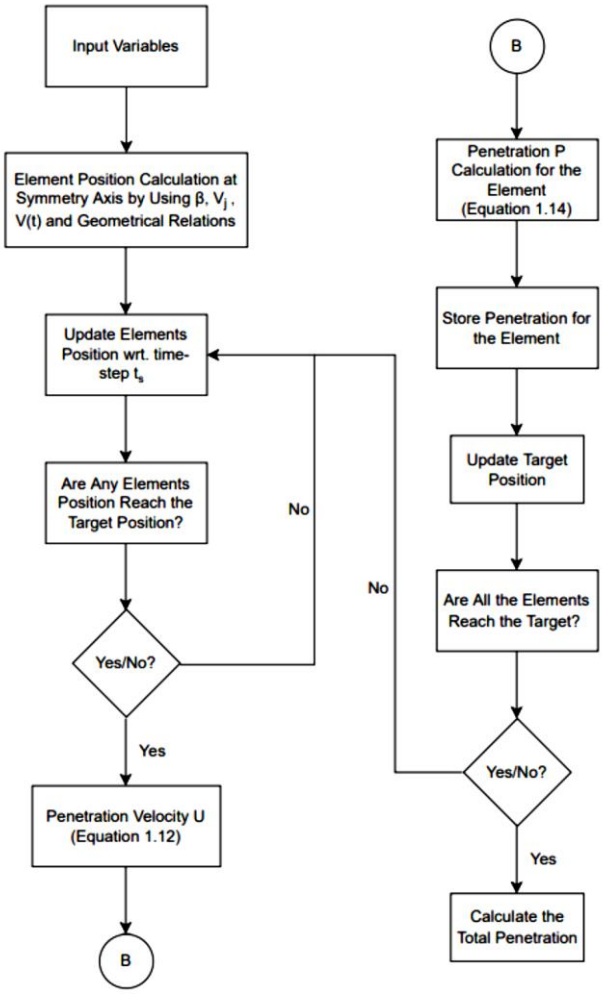

Figure 4-7 Flow Chart of Analytical Code for Jet Penetration Flow

According to selected design parameters (especially for the small stand-off distance), elements may start to penetrate before all the elements reach to symmetry axis. This situation disrupts two stages approach (jet formation and penetration) of the code. So, the MATLAB code separates the jet elements which have not reached the symmetry axis yet due to their positions on the liner and their collapse velocities. Then these elements treated seperately as a second group. So, the penetration calculation continues from the position where the last element of the first group penetrates to target.

During the analytical calculations, it is examined that the jet break-up times are significantly larger than the time when all the elements are deleted and the

penetration ends. So, jet break-up formula is not included in the code. But at Section 5, accuracy of the formula is tested by comparing the break-up time results with AUTODYN simulations and consistent results are achieved.

Analytical jet formation and penetration MATLAB code is shared at Appendices-A.

4.5 Comparison of Analytical Code Penetration Results with Experiments

Developed MATLAB code has been run for the LSC/CLSC configurations for the firing experiments for which the details are given in Section 3. R_t and Y_p values are selected according to Rosenberg and Dekel study (mentioned in reference [21]). They suggest the use of a yield stress factor of 4-5 for aluminum targets, and a factor of 5-6 for steel targets. α constant is determined by fitting the penetration results of the prototype #5 and #8 of CLSC (On Plane) configuration. Then, the determined α value constant is used for the analytical penetration calculations of other prototypes of CLSC (On Plane), LSC and CLSC (On Tube of Inner Radius) configurations. Element number n and time step t_s are selected as 300 and 0.1 μs, respectively. It is observed that larger n, smaller t_s values have not a significant effect on the penetration results.

Analytical theory assumes the ideal case for the LSC/CLSC penetration, so the code results are compared with the maximum penetrations of the experiment configurations. Factors like explosive homogeneity, efficient initiation of explosive, liner tolerances (for example thickness variance and offsetting from symmetry axis), target hardness variance are neglected which are the possible reasons for the penetration variance in the experiments.

4.5.1 Fitting Constant α to Penetration Data

α constant is determined as 0.0092 by fitting the penetration results of the prototype #5 and #8 of CLSC (On Plane) configuration.

4.5.2 LSC Configuration

LSC configurations analytical code results and their comparison with experiments are given at Table 4-3. R_t, Y_p, and α values are given at Table 4-4. According to the analytical code results, experiments are simulated with errors of %21.6 and %18.1 for prototypes #1 and #2, respectively.

Table 4-3 LSC Configurations Analytical Code Results and Their Comparison with Experiments

Prototype #	**M/C Ratio**	**Stand-off Distance (mm)**	**Experiment Maximum Penetration (mm)**	**Analytical Code Penetration (mm)**	**Error With Respect to Experiment (%)**
1	0.8	10	12.5	15.2	21.6
2		15	15.4	18.2	18.1

Table 4-4 R_t, Y_p, and α Values for LSC Configurations Analytical Code

Related Constant	**Corrected Value**
R_t	2
Y_p	0.8
α	0.0092

4.5.3 CLSC (On Plane) Configuration

CLSC (On Plane) configurations analytical code results and their comparison with experiments are given at Table 4-5. R_t, Y_p, and α values are given at Table 4-6. According to analytical code results, experiments are simulated with a maximum error of %9.3 .

Table 4-5 CLSC (On Plane) Configurations Analytical Code Results and Their Comparison with Experiments

Prototype #	M/C Ratio	Stand-off Distance (mm)	Experiment Maximum Penetration (mm)	Analytical Code Penetration (mm)	Error With Respect to Experiment (%)
2	1.06	17	10.0	9.3	7
3		22	11.0	10.5	4.5
5	0.94	17	11.1	10.9	0.9
8		22	11.5	11.6	0.9
10	0.84	17	12.7	12.6	0.8
12		22	12.7	13.2	4
14	0.65	17	15.0	16.4	9.3
15		22	16.7	17.4	4.2

Table 4-6 R_t, Y_p, and α Values for CLSC (On Plane) Configurations Analytical Code

Related Constant	Corrected Value
R_t	3.8
Y_p	0.8
α	0.0092

4.5.4 CLSC (On Tube of Inner Radius) Configuration

CLSC (On Tube of Inner Radius) configurations analytical code results and their comparison with experiments are given at Table 4-7. Since all the targets are cut completely, maximum penetration is unknown, so target thickness column is added to Table 4-7 instead of maximum penetration for the experiments. R_t, Y_p, and α values are given at Table 4-8.

Table 4-7 CLSC (On Tube of Inner Radius) Configurations Analytical Code Results and Their Comparison with Experiments

Prototype #	**M/C Ratio**	**Stand-off Distance (mm)**	**Target Thickness (mm)**	**Analytical Code Penetration (mm)**
1	0.8	12	28	26.1
2		15	25	27.7
3		18	22	28.7
4		21	19	30.7

Table 4-8 R_t, Y_p, and α Values for CLSC (On Tube of Inner Radius) Configurations Analytical Code

Related Constant	**Corrected Value**
R_t	2
Y_p	0.8
α	0.0092

CHAPTER 5

SIMULATION OF CIRCULAR LINEAR SHAPED CHARGE AND COMPARISON WITH EXPERIMENTS

Numerical simulations of LSC/CLSC test configurations are carried out in AUTODYN software. Simulations are done in 2D, plane symmetry is selected according to symmetry axis of LSC/CLSC by considering the geometry of designs.

5.1 CLSC Modelling and Mesh Sensitivity Study

Prototype #10 from CLSC (On Plane) experiment is selected as a sample for the modelling process. The explosive, casing, liner, and target are formed in a Lagrange solver and then filled in a Euler space which is formed as air. Then, all the simulations are run in Euler solver. 2-D model of the sample is shown in Figure 5-1.

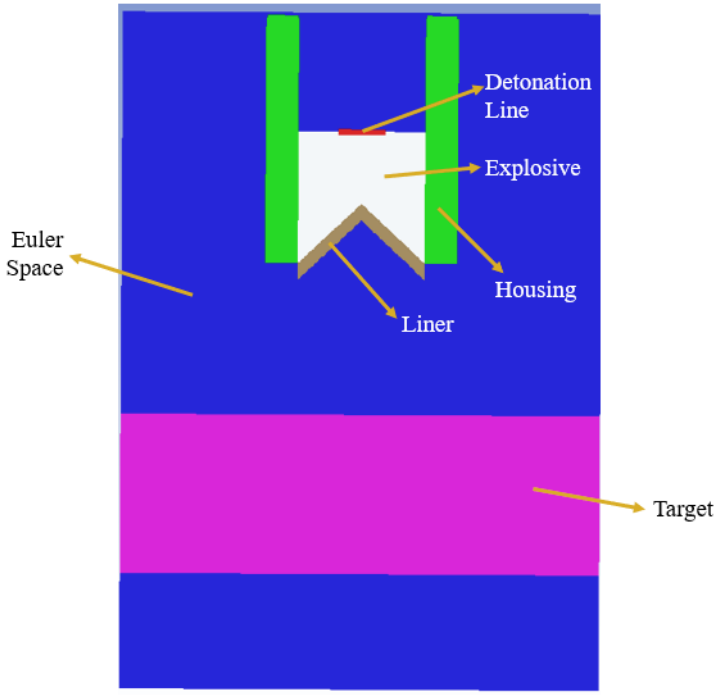

Figure 5-1 CLSC (On Plane) Model Sample

Material models of the parts are given at Table 5-1. All the material models are selected from AUTODYN material library. LX-04 is selected as an explosive because of its close explosive content (%85 HMX, %15 binder) to PBX-110 (%88 HMX, %12 binder). Exceptionally, density of the explosive LX-04 is selected as 1.65 g/cm^3 and the detonation velocity is changed to 7790 m/s which are the measured values of the used PBX-110 before starting the experiments.

Table 5-1 CLSC Material Model Which is Used for Simulation Model Development

Part	**Material Model**	**Equation of State**	**Strength Model**
Explosive	LX-04	JWL	None
Liner	Cu-OFHC	Shock	Steinberg-Guinan
Casing	Aluminum 6061-T6	Shock	None
Target	Stainless Steel	Shock	Piecewise-Johnson Cook
Space	Air	Ideal Gas	None

After modelling the prototype, a mesh sensitivity study is done for the model. On the meshing process, model is classified into 2 regions which are the action zone and transition zone. Action zone is considered as the region where the jet formation and penetration occur. Smallest and constant meshes are formed for this area. On the other hand, the regions where the jet formation and penetration are not significant is named as transition zone. Transition zone is designed in such a way that, as the distance between the element in the transition region and the action zone surface gets larger, mesh dimensions also get larger. By enlarging the mesh sizes of the transition zone, it is aimed to reduce the total number of meshes so to run the simulations quicker by reducing the computation time. Action zone and transition zone are shown in Figure 5-2 on CLSC (On Plane) model.

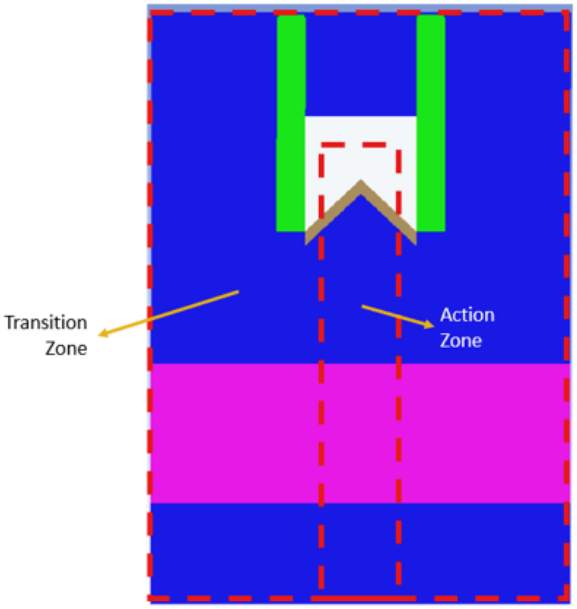

Figure 5-2 Action Zone and Transition Zone at CLSC (On Plane) Model

Mesh distribution on CLSC and target for a 0.15 mm mesh size is shown in Figure 5-3 and Figure 5-4, respectively. From the related figures, as the meshes move away from the action zone, the increase in mesh sizes can be observed.

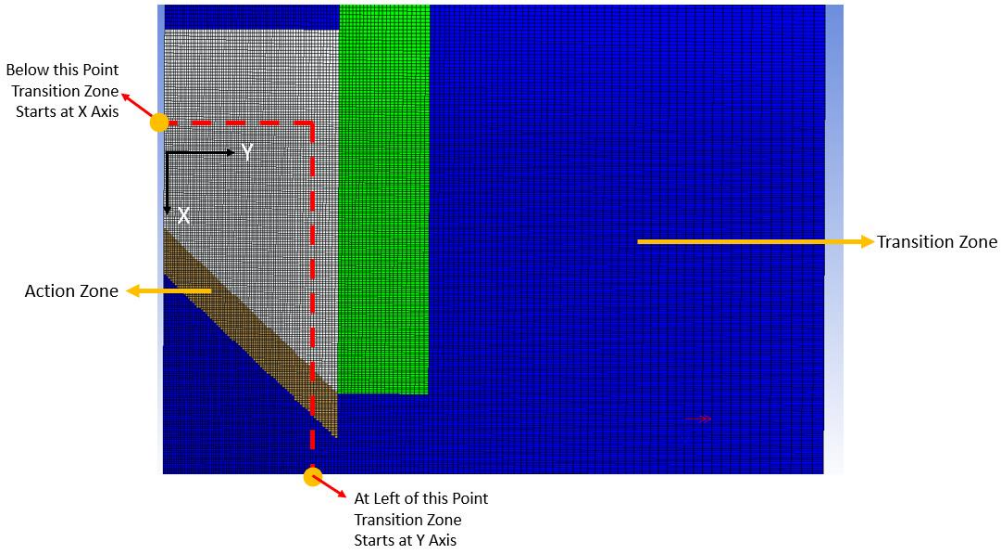

Figure 5-3 Mesh Distribution on CLSC at Action Zone and Transition Zone for a 0.15 mm Mesh Size

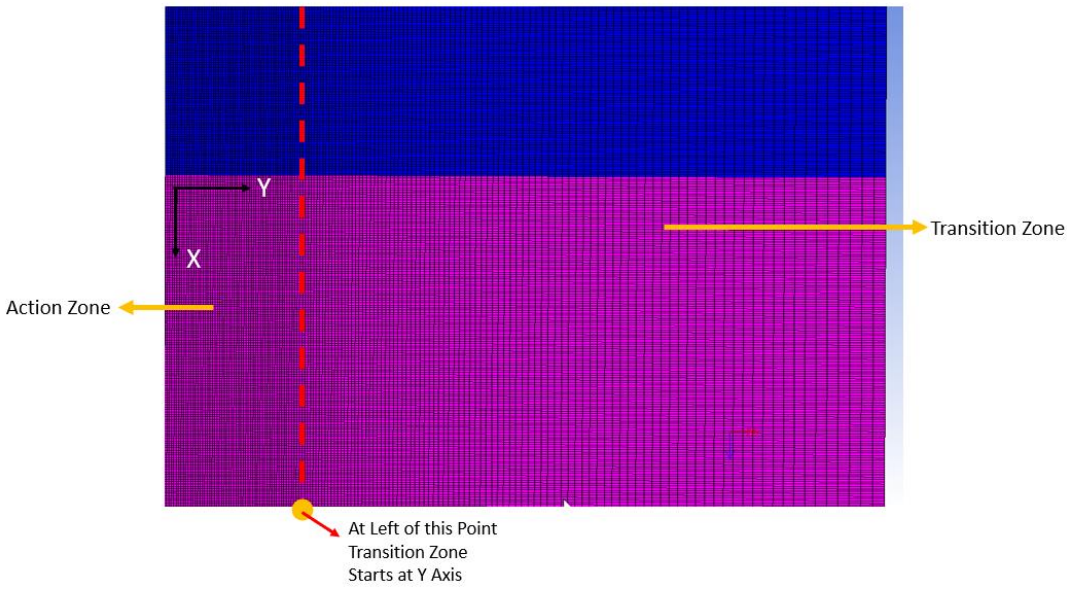

Figure 5-4 Mesh Distribution on Target at Action Zone and Transition Zone for a 0.15 mm Mesh Size

To examine the mesh size sensitivity of the model, three different spaces are formed for different cell sizes which are 0.15 mm, 0.1 mm, and 0.05 mm (It should be noted that the given cell sizes are for the action zone mesh dimensions). Explosive is initiated from its open surface with a 6 mm detonation line (See Figure 5-1 for the detonation line view). The length of the detonation line is selected considering the detonator diameter which is used in the experiments. For the liners, position versus velocity data is obtained at t=10 µs and compared for different cell sizes. According to related data, the liner velocity gets stable for cell sizes smaller than 0.1 mm. So, the LSC/CLSC experiments are simulated by using 0.1 mm mesh cell size for the action zone. Total number of cells for the simulations which are used in mesh sensitivity analysis are given at Table 5-2. Jet velocity versus position plot at t=10 µs for different cell sizes are shown in Figure 5-6. In the related figure, 8 mm position interval is compared for the different cell sizes. x=8 mm is the tip of the jet and x=0 mm is the distance from the jet tip which is 8 mm. These related positions on the jet are shown in Figure 5-5 which is taken at t=10 µs from AUTODYN simulation.

Table 5-2 Mesh Sensitivity Analysis Total Cell Number for Different Cell Sizes

	0.05 mm	**0.1 mm**	**0.15 mm**
Total Cell Number	300,000	75,000	33,300

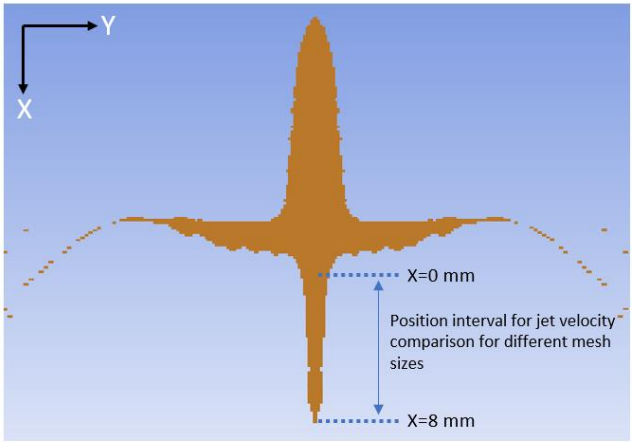

Figure 5-5 Position Interval for Jet Velocity Comparison for Different Mesh Sizes

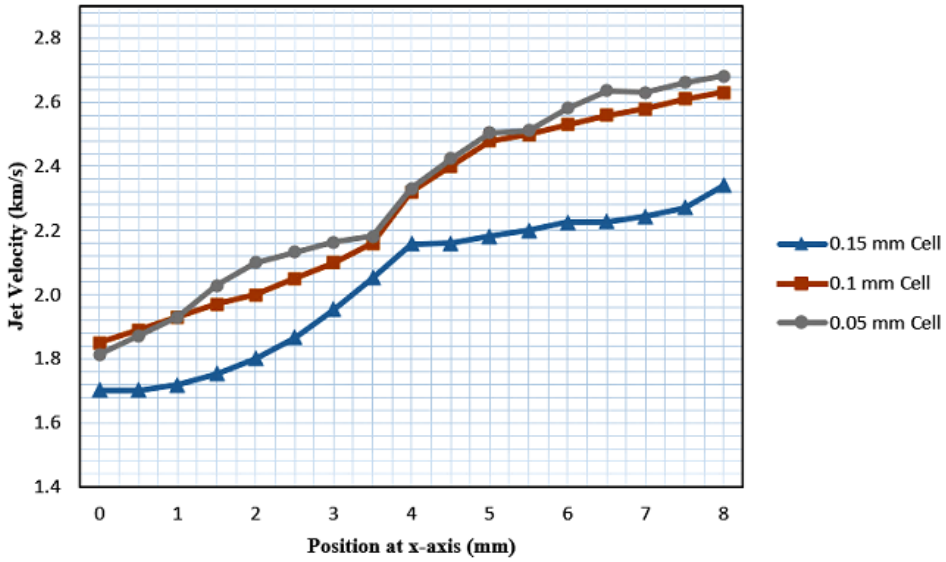

Figure 5-6 Position versus Jet Velocity Plot at t=10 µs for Different Cell Sizes

To verify the approach of the simulation modelling, position versus velocity data of the 0.1 mm cell size simulation is also compared with the analytical code position versus velocity data at t=10 µs. According to the simulation results, jet velocity is

deviated maximum of %8 from the analytical code results. Position versus velocity plot at t=10 μs for 0.1 mm cell size simulation and analytical code is shown in Figure 5-7:

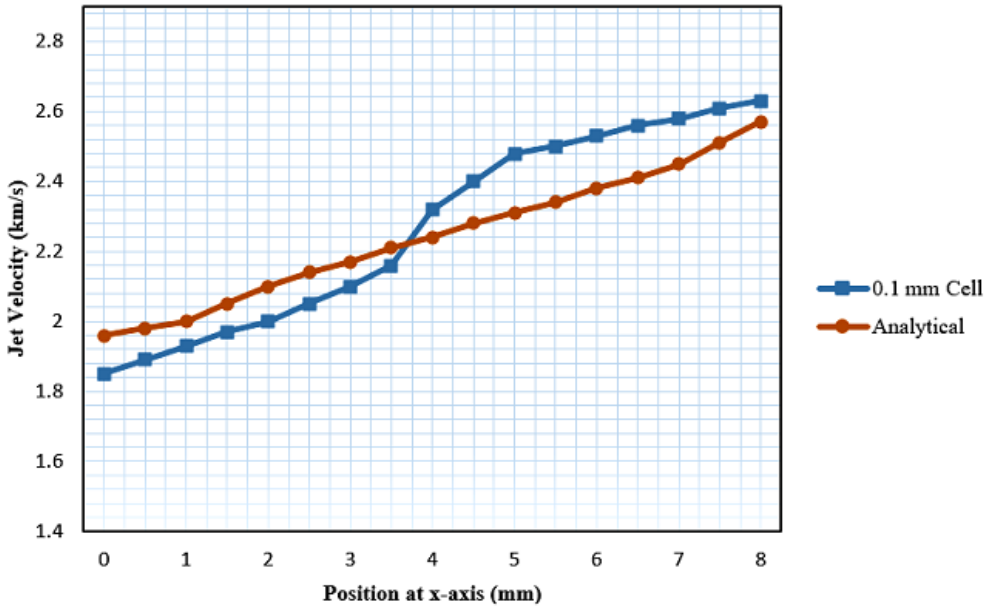

Figure 5-7 Comparison of Jet Velocity of 0.1 mm Cell Size Simulation and Analytical Solution

5.2 Comparison of Simulations with Experiments

LSC/CLSC experiments are simulated by the 0.1 mm cell size models. The material models and the penetration results of simulations are given in below sections. The penetration results of simulations are compared with the experiments and analytical code results. AUTODYN simulation images are also shown in figures.

5.2.1 LSC Simulations

LSC experiments are simulated by using the material model which is given at Table 5-3.

Table 5-3 Material Model of LSC Simulations

Part	Material Model	Equation of State	Strength Model
Explosive	LX-04	JWL	None
Liner	Cu-OFHC	Shock	Steinberg-Guinan
Target	Aluminum 7075-T6	Shock	Steinberg-Guinan
Space	Air	Ideal Gas	None

The penetration results of the simulations are given at Table 5-4. The percentage deviations of these results, with respect to the results of analytical codes and experiments, are also given in the same table. These results show that the penetration errors with respect to the analytical code are 8% and 3.4% for prototypes #1 and #2, respectively. But also, acceptable errors (12% and 20.1%) are found with respect to experimental results.

Table 5-4 LSC Simulation Penetration Results and Errors with respect to Analytical Code Results and Experiments

Prototype #	M/C Ratio	Stand-off Distance (mm)	Simulation Penetration (mm)	Error with respect to Analytical Code Penetration (%)	Error with respect to Experiment Maximum Penetration (%)
1	0.8	10	14	8	12
2		12.5	18.5	3.4	20.1

Formation of the jet, penetration into the aluminum target and the view of the target after the penetration are shown in Figure 5-8 for the prototype #2.

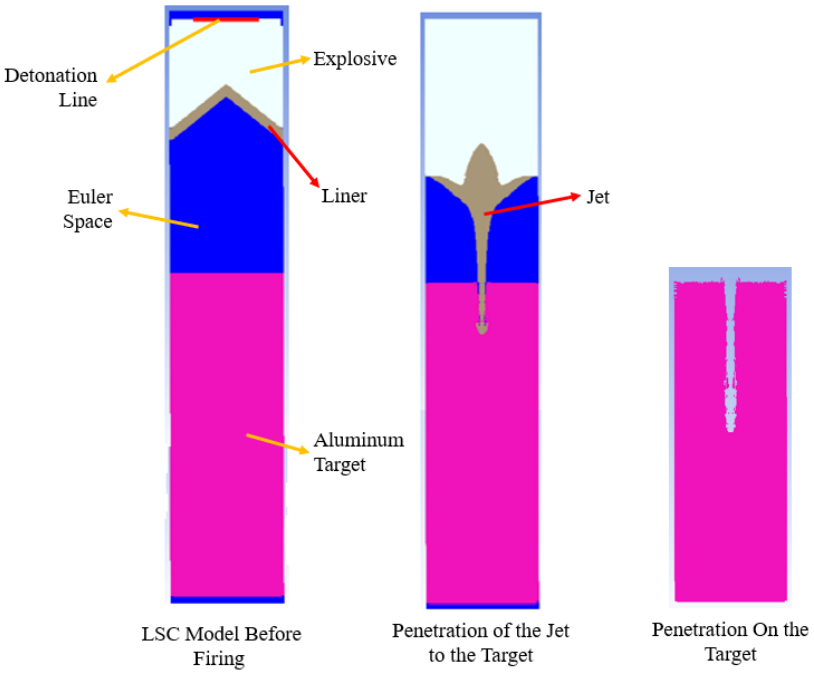

Figure 5-8 LSC Simulation Figures

5.2.2 CLSC (On Plane) Simulations

CLSC (On Plane) experiments are simulated by using the material model which is given at Table 5-5. In this section, differently from LSC simulations, another two alternative liner models are also simulated to examine the effect of liner model selection for penetration.

Penetration results of the simulations and their variance from the experiments for the liner alternative 1 are shared at Table 5-6.

Table 5-5 Material Model of CLSC (On Plane) Simulations

Part	Material Model	Equation of State	Strength Model
Explosive	LX-04	JWL	None
Liner Alternative 1	Cu-OFHC	Shock	Steinberg-Guinan
Liner Alternative 2	Cu-OFHC	Linear	Johnson-Cook
Liner Alternative 3	COPPER	Shock	Piecewise-Johnson Cook
Target	Stainless Steel	Shock	Piecewise-Johnson Cook
Housing	Aluminum 6061-T6	Shock	Steinberg-Guinan
Space	Air	Ideal Gas	None

Table 5-6 CLSC (On Plane) Simulation Penetration Results and Errors with respect to Analytical Code Results and Experiments for Liner Alternative 1

Prototype #	M/C Ratio	Stand-off Distance (mm)	Simulation Penetration (mm)	Error With Respect to Analytical Code Penetration (%)	Error With Respect to Experiment Maximum Penetration (%)
2	1.06	17	9.5	9.2	5
3		22	9.9	1	10
5	0.94	17	10.8	0.9	2.7
8		22	11.1	0.9	3.5
10	0.84	17	12.3	0.8	3.1
12		22	12.2	9.3	4
14	0.65	17	14.2	11.3	5.4
15		22	15.5	8.9	7.2

Penetration results of the simulations and their variance from the experiments for the liner alternative 2 are shared at Table 5-7.

Table 5-7 CLSC (On Plane) Simulation Penetration Results and Errors with respect to Analytical Code Results and Experiments for Liner Alternative 2

Prototype #	**M/C Ratio**	**Stand-off Distance (mm)**	**Simulation Penetration (mm)**	**Error with respect to Analytical Code Penetration (%)**	**Error with respect to Experiment Maximum Penetration (%)**
2	1.06	17	9.9	13.8	0.1
3		22	10.3	5.1	6.4
5	0.94	17	10.6	1	4.5
8		22	10.7	2.8	7
10	0.84	17	12.6	3.3	0.8
12		22	11.4	13	11.3
14	0.65	17	12.5*	22	16.7
15		22	16.5	3	1.2

*The simulation cannot be completed because of the small time step error.

Penetration results of the simulations and their variance from the experiments for the liner alternative 3 are shared at Table 5-8.

For all three liner alternatives, reasonable penetration results are obtained by using simulation, with respect to analytical code and experiments. Smallest errors are founded for liner alternative 1. Formation of the jet, penetration into the aluminum target and view of the target after the penetration is given in Figure 5-9 for the prototype #10.

Table 5-8 CLSC (On Plane) Simulation Penetration Results and Errors with respect to Analytical Code Results and Experiments for Liner Alternative 3

Prototype #	M/C Ratio	Stand-off Distance (mm)	Simulation Penetration (mm)	Error With Respect to Analytical Code Penetration (%)	Error With Respect to Experiment Maximum Penetration (%)
2	1.06	17	9.7	11.5	3
3		22	10.5	7.1	4.5
5	0.94	17	10.4	2.8	6.4
8		22	10.6	3.7	7.8
10	0.84	17	11.1	9.1	12.6
12		22	11.4	13.7	10.2
14	0.65	17	12	25	20
15		22	14.7	13.6	12

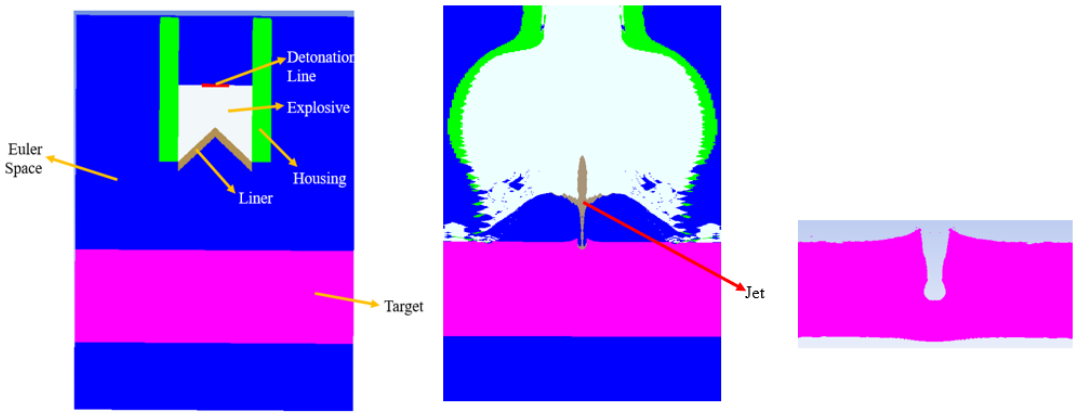

Figure 5-9 CLSC (On Plane) Simulations

5.2.3 CLSC (On Tube of Inner Radius) Simulations

CLSC (On Tube of Inner Radius) experiments are simulated by using the material model is given at Table 5-9.

Table 5-9 Material Model of CLSC (On Tube of Inner Radius) Simulations

Part	Material Model	Equation of State	Strength Model
Explosive	LX-04	JWL	None
Liner	Cu-OFHC	Shock	Steinberg-Guinan
Housing	Aluminum 6061-T6	Shock	Steinberg-Guinan
Target	Aluminum 7075-T6	Shock	Steinberg-Guinan
Space	Air	Ideal Gas	None

Penetration results of the simulations and their variance from the experiments are given at Table 5-10.

Table 5-10 CLSC (On Tube of Inner Radius) Simulation Penetration Results and Errors with respect to Experiments

Prototype #	M/C Ratio	Stand-off Distance (mm)	Experiment Maximum Penetration (mm)	Simulation Penetration (mm)
1	0.8	12	No penetration results since all the targets are cut completely.	All the targets are cut completely.
2		15		
3		18		
4		21		

Formation of the jet, penetration into the aluminum target and view of the target after the penetration is given in Figure 5-10 for the prototype #1.

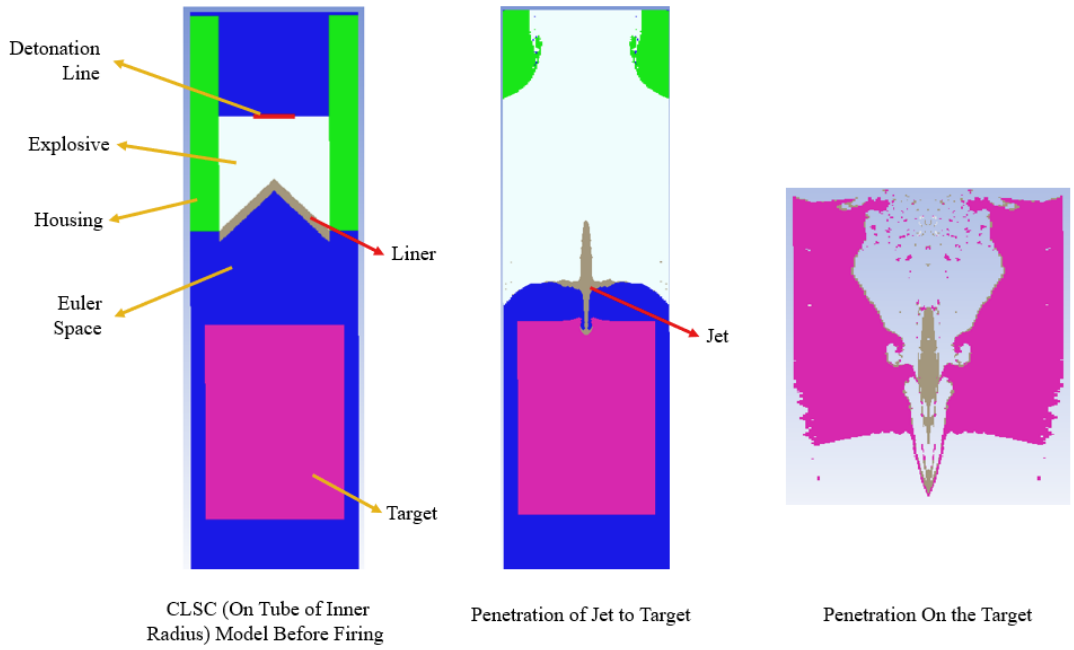

Figure 5-10 CLSC (On Tube of Inner Radius) Simulations

5.3 Comparison of the Jet Break Results of Simulations and Analytical Codes

AUTODYN model of Prototype #10 from CLSC (On Plane) configuration is initiated in a new simulation after removing the target from it. By removing the target, it is aimed to permit the jet to stretch sufficiently so that the jet break-ups can be observed. According to simulation, jet break-up starts to form at t=34 μs after the initiation of CLSC. Additional jet break-ups continue to occur at different regions of the jet as the simulation time increases. First few jet break-ups are shown at different simulation times in Figure 5-11.

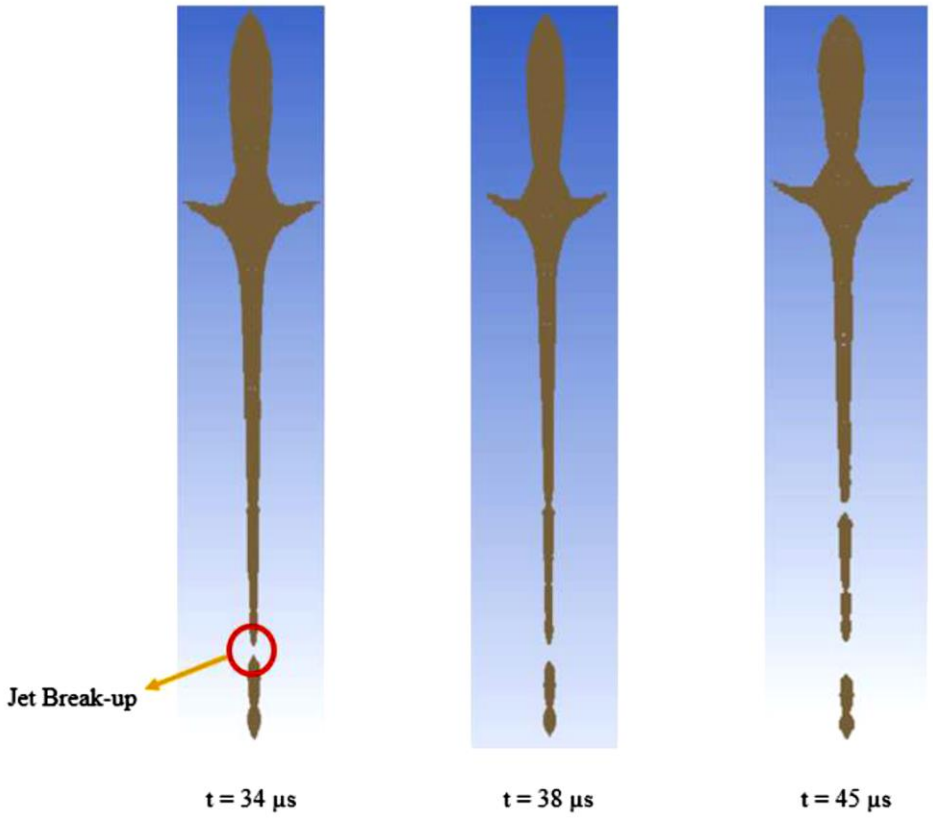

Figure 5-11 CLSC (On Plane) Prototype 10, Jet Break-up Figures at Different Simulation Times

For the prototype #10, jet break-up time is also calculated analytically by using equation 1.10 in MATLAB. The jet break-up time using analytical approach is founded as 38 µs.

CHAPTER 6

DISCUSSION AND CONCLUSION

6.1 Discussion and Conclusion

In this thesis study, three different Linear Shaped Charge (LSC) configuration have designed, produced, and tested to cut specific targets. In the first design, a LSC is designed to cut linear targets. A straight V shaped copper liner is manufactured. Then, a plastic bonded explosive is assembled on the liner. The LSC is fired from different stand-off distances and penetrates aluminum target 13.3 mm on average. In the second and third configurations, a new design which is called Circular Linear Shaped Charge (CLSC) is introduced which can be an alternative to Flexible Linear Shape Charge (FLSC) in specific cases. A circular V shaped copper liner and an aluminum housing is manufactured and assembled by bolts. Then, molten PBX-110 explosive is poured on the assembly and cured inside. CLSCs are designed in such a geometry that when they are initiated configuration can cut the targets in circular plane and tube profile. They are classified as CLSC (On Plane) and CLSC (On Tube of Inner Radius) in themselves. CLSC (On Plane) prototypes with different explosive masses are fired from different stand-off distances and cut steel targets up to 14.9 mm on average. In the same way, CLSC (On Tube of Inner Radius) prototypes are fired from different stand-off distances and cut 19 to 28 mm aluminum targets completely. By these experiments, it is shown that cutting of the specific profiles can also be done by manufacturing rigid metal parts by considering the target geometry and filling it with molten explosive which can be an alternative to FLSC. This method can be more advantageous than FLSC especially for following conditions:

- The target profiles are smaller than the FLSC bend radius.
- FLSC penetration is insufficient for the target thickness.

In Chapter 4, theoretical formulas for jet formation and penetration are investigated. An analytical code is written by using these formulas. Then, the penetration values of the experiment prototypes given in Chapter 3 are calculated by using the analytical code mentioned in Chapter 4. Close results are obtained with experiments.

In the Chapter 5, a 2D AUTODYN model is formed for LSC/CLSC designs. For a sample prototype, the velocities of the jet elements are found by using the simulations and analytical codes, then compared with each other. It is seen that the jet velocities are coherent with each other. Then, experiment prototypes are simulated by using this model and convenient penetration results are obtained. From the simulations, it is seen that the selection of the material model for copper directly affects the penetration and so the accuracy with the experiments. According to results, using Steinberg-Guinan material model for the copper reveals the closest results with the experiments. In the study, jet break-up times of a sample prototype is also investigated by using the simulations and analytical code. For the beginning of the break-up time, remarkably close results are obtained for the related two approaches.

In this study, LSC/CLSC jet formation and penetration are modeled analytically with MATLAB codes and numerically with AUTODYN simulations by a good accuracy. However, it should be noted that both two approaches have disadvantages and they should be used together to get accurate results for different designs. During the penetration, analytical approach considers only hydrodynamic penetration (the strength and viscosity of materials are neglected) but at lower jet velocities this theory does not hold. So, a correction factor (α value from Pack-Evans formula, Equation 1.14) is needed to determine penetration more accurately. This correction factor is determined according to experiments or simulation results. On the other hand, tumbling and dispersion effects of the broken jets do not count while simulating the penetration in AUTODYN. So even the jet break-up happens, the broken jet continues to penetrate the target. To get consistent results with experiments, the jet break-up time of the design should be calculated analytically and penetrations after the break-up time should be examined carefully.

6.2 Future Work

The study can also be improved in different ways which are listed below:

- Jet-break up formulas should be included into the analytical code for higher stand-off distances.
- Broken jet penetrations can be simulated by implementing Pseudorandom Number Generator (PRNG) algorithm to the analytical code. The algorithm can be taken into consideration for the LSC/CLSC experiments which are fired at high stand-off distances.
- Effect of the liner tolerances and explosive density variance to penetration may be investigated by analytic and numeric models.

REFERENCES

[1] V. Slavica, M. Dobrilovic, and V. Skrlec, "The Efficiency of Linear Shaped Charges," *Technical Gazette,* vol. 21, pp. 525-531, 2014.

[2] Held, M. "Liners for Shaped Charges," Journal of Battlefield Technology, vol. 4, pp. 1-5, 2001.

[3] Accurute Energetic Systems, Linear Shaped Charge [Exhibition Catalogue].

[4] Guangyu. "Microsturucture and mechanical properties of tin-based alloys for miniature detonating cords (Ph.D. Thesis)," Brunel University London, 2019.

[5] D. Novetny, and M. Malery, "Historical Development of Linear Shaped Charge," Joint Propulsion Conference & Exhibit, vol. 43, pp. 4-12, 2007.

[6] Gazonas, Segletes, Paxton, Gardiner, "Hydrocode Simulation of Flexilinear Shaped Charge Jet Penetration Into an Explosive Filled Cylinder," Army Research Laboratory, 1996.

[7] Ö. Ender, "Kesme Tekniklerinde Kullanılan Doğrusal Boşluklu Patlayıcı Kaplarında Optimum Ayak Mesafelerinin Araştırılması (M.S. Thesis)," Türkiye Cumhuriyeti Ankara Üniversitesi Sağlık Bilimleri Enstitüsü, 2006.

[8] W. C. Davis, "The Detonation of Explosives," Scientific American, vol. 256, pp. 106-113, 1987.

[9] M. Ortell, "A Modified Initiation and Cut Profile Study of the 10500 Grain Per Foot Linear Shaped Charge (M.S. Thesis)", Missouri University of Science and Technology, 2014.

[10] Y. Wenbo, and J. Gulkey, 1964. "Shaped Charge Liner," United State Patent 2013/0340643. 1964.

[11] S. Dusan, “Optimization of the Production Process, Characterization and Efficiency of a Linear Detonation Shaped Charge with a Small Linear Mass of the Explosive Core,” Scientific Technical Review, vol. 65, pp. 23-30, 2015.

[12] A. C. Schwarz, “Application of Hexanitrostilbene (HNS) in Explosive Components,” Sandia Laboratories, 1972.

[13] R. F. Hatfield, “Process of Making Linear Shaped Charge Explosive Devices,” United State Patent 3,138,054, 1964.

[14] Mondial Defence Systems. Semtex RAZOR, Flexible Linear Shaped Charge [Exhibition Catalogue].

[15] Chemring Energetic UK. SABREX Flexible Linear Shaped Charge [Exhibition Catalogue]. Ardeer Site, Stevenston, UK: Ayrshire KA20 3LN.

[16] Wang, Xiong, Chen, Fan, “A Linear Shaped Charge Neutron Radiography Precise Detection Scheme,” Journal of Theoretical and Applied Information Technology, vol 46, 2012.

[17] Miyoshi, Ohba, Kitamura, Inoue, Hiroe, “Improvement of penetration performance of linear shaped charges,” WIT Transactions on State of the Art in Science and Engineering, vol 75, 2014.

[18] G. Huanwen, Z. Xu, and S. Wenjuan, “Experiment Study on the Performance of Explosive Cutting,” 50th AIAA/ASME/SAE/ASEE Joint Propulsion Conference, 2014.

[19] Burch, “Determining and mitigating the effects of firing a linear shaped charge under water (M.S. Thesis),” Missouri University of Science and Technology, 2014.

[20] A. S. Gözübüyük, “Factors Affecting the Penetration due to a Shaped Charge (M.S. Thesis),” Middle East Technical University, 2005.

[21] M. Johnston, and S. Lim, “Numerical Observation of the Jet Flight Patterns of Linear Shaped Charges,” Appl. Sci., vol. 2, pp. 629-640, 2012.

[22] Kim, Madsen, Pincay, Al-Shebab, Baker, “Application of Linear Shaped Charges For Warhead Venting,” 23rd International Symposium on Ballistics Tarragona, 2007.

[23] E. Gürel, “Modeling and Simulation of Shaped Charges (M.S. Thesis),” Middle East Technical University, 2009.

[24] Ç. G. Bingöl, “Deformation Effects of Straight Segment of FLSC to Nearby Plates Due to Varying Backspace Distance (M.S. Thesis),” Middle East Technical University, 2004.

[25] E. Baker, “Modeling and Optimization of Shaped Charge Liner Collapse and Jet Formation,” Washington State University, 1992.

[26] W. Walters and J. Zukas, Fundamentals of shaped charges, New York: John Wiley &Sons, 1989.

[27] J. T. Dehn, “Models of Explosively Driven Metal,” US Army Ballistic Research Laboratory, 1984.

[28] E. M. Pugh, J. Eichelberger, and N. Rostoker, “Theory of Jet Formation by Charges with Lined Conical Cavities,” Journal of Applied Physics, vol. 23, no. 2, 1952.

[29] S. Y. Mohamed, A. M. Riad, Y. Kresha, “Penetration of a Shaped Charge Jet Into a Metallic Target,” 9st ASAT Conference, 2001.

[30] M. J. Murphy, “Explosives with Lined Cavities,” University of California, 1983.

[31] W.J. Jiao, X.W. Chen, “Approximate solutions of the Alekseevskii-Tate model of long-rod penetration,” Acta Mechanica Sinica, vol. 34, pp. 334-348, 2018.

[32] W. Walters, “Introduction to Shaped Charges,” Army Research Laboratory, 2007.

APPENDICES

A. Analytical Solution MATLAB Code

```
clear all
close all
clc

format short

%Inputs: %All the time parameters are in microsecond unit in the code.

alphadegree = 45; %Apex Angle
alpha = deg2rad(alphadegree);

linerlenght = 8; %Lenght of the liner in the x-axis from apex to base

n = 50; %Element number

ts = 0.1;

L = 2.1 %Liner Thickness

E = 2.9; %Gurney velocity for HMX E=2.9 km/s (from literature)

LM = 0.84; %M/C ratio
SS = 26;

RoT = 7.9; %Target Density
RoP = 8.9; %Penetrator Density
Rt = 3.8  %Target Resistance
Yp = 0.8 %0.2*4; %Penetrator Resistance

AA = 0.5 %Patrick-Evans Penetration Formula Constant((alpha*Y)/pj)
Ucut= 0.5;

for a = 1:n

   X(a)=linerlenght*((a-1)/n); %X: element position at X coordinate
                %a: element number

   Y(a)=tan(alphadegree)*X(a); %X: element position at X coordinate
                %a: element number
```

```
end  %calculating the position(X,Y) of the elements


for a = 1:n

   u(a)=LM*n/(n-a+1); %u:M/C ratio for different elements

end


E = 2.9; %Gurney velocity for HMX E=2.9 km/s
D=7.790; %Detonation velocity
Udet = D/sin(alpha);

j = 0;

syms uu

V0diffwrtLM = 0.36.*D.*atan(2./(3.*uu));
diffV0u = diff(V0diffwrtLM,uu);

for a = 1:n

    V0(a) = 0.36*D*atan(2/(3*u(a))); %Trinks Collapse Velocity Formula

    delta(a) = asin(V0(a)*cos(alpha)/(2*Udet));
    deltadegree(a) = rad2deg(delta(a));

    betaplus(a) = alpha+(2*delta(a)); % "steady-state" collapse angle
    betaplus(a) = wrapTo2Pi(betaplus(a));

    diffV0(a) = (-231/(125*u(a)^2*(4/(9*u(a)^2)+1)))*(LM/7.5);

    beta(a) = atan((sin(betaplus(a))-(X(a)*sin(alpha)*(1-
tan(alpha+delta(a))*tan(delta(a)))*diffV0(a)/V0(a)))...

/((cos(betaplus(a))+(X(a)*sin(alpha)*(tan(alpha+delta(a))+tan(delta(a)))*diffV0(a)/
V0(a)))));
    beta(a) = wrapTo2Pi(beta(a));
    betadegree(a) =rad2deg(beta(a));

    % Jet and Slug Velocity Calculation

    Vj(a) = (V0(a)*cos(alpha+delta(a)-(beta(a)/2)))/sin(beta(a)/2);
```

```
    Vslug(a) = (V0(a)*cos(alpha+delta(a)-(beta(a)/2)))/cos(beta(a)/2);

end

Vpl = 0.15; %Plastic Velocity
z=0;
m=1;

for a = 1:n

    AP(a) = sqrt((X(a))^2+(Y(a))^2);
    Xn(a) = AP(a)*sin((pi/2)+delta(a))/sin(90-alpha-delta(a));
    A(a) = sqrt((X(a)-Xn(a))^2+(Y(a))^2);
    t(a) = A(a)/(V0(a)); %travelling time to y=0 in µs
    t0(a) = a/n*linerlenght/Udet; %sweep velocity delay in µs
    tau = 0.5;
    Vc(a) = V0(a)*(1-exp(-(t(a)-t0(a))/tau)); %Corrected Collapse Velocity

    delta(a) = asin(Vc(a)*cos(alpha)/(2*Udet));
    deltadegree(a) = rad2deg(delta(a));

    betaplus(a) = alpha+(2*delta(a)); % "steady-state" collapse angle
    betaplus(a) = wrapTo2Pi(betaplus(a));

    diffV0(a) = (-231/(125*u(a)^2*(4/(9*u(a)^2)+1)))*(LM/7.5)*(1-exp(-(t(a)-
t0(a))/tau));

    beta(a) = atan((sin(betaplus(a))-(X(a)*sin(alpha)*(1-
tan(alpha+delta(a))*tan(delta(a)))*diffV0(a)/V0(a)))...

/((cos(betaplus(a))+(X(a)*sin(alpha)*(tan(alpha+delta(a))+tan(delta(a)))*diffV0(a)/
V0(a)))));
    beta(a) = wrapTo2Pi(beta(a));
    betadegree(a) =rad2deg(beta(a));
    betaplusdegree(a) =rad2deg(betaplus(a));

    if n*0.72 < m && m < n*0.89

        betadegree(a) = 62+ 10*(a-(n*0.72));
        beta(a) = deg2rad(betadegree(a));
        z = z+1;

    end

    if n*0.89 < m
```

```
        betadegree(a) = 72+ 10*(a-(n*0.89));
        beta(a) = deg2rad(betadegree(a));

    end

    Xn(a) = AP(a)*sin((pi/4)+beta(a))/sin(90-beta(a));
    A(a) = sqrt((X(a)-Xn(a))^2+(Y(a))^2);
    t(a) = A(a)/(Vc(a)); %corrected travelling time to y=0 in µs

    % Corrected Jet and Slug Velocity Calculation

    Vjnew(a) = (Vc(a)*cos(alpha+delta(a)-(beta(a)/2)))/sin(beta(a)/2);
    Vslugnew(a) = (Vc(a)*cos(alpha+delta(a)-(beta(a)/2)))/cos(beta(a)/2);

    if Vjnew(a)>2.5 && a > 0.6*n

        Vjnew(a) = 0;

    end

    m = m+1;
end

p=0;
for a = 1:n/2

  if Vjnew(a) == max(Vjnew)

      p = a;
      break;

  end

  m(a) = 2*3.14*a;
  Vjdmj(a) = Vjnew(a)*m(a);
  dmj(a) = m(a);

end

Vtip = sum(Vjdmj)/sum(dmj); %Corrected Jet tip Velocity
m=0;

for a = 1:n
```

```
    if Vjnew(a) > Vtip

      m1 = a;

         break;


    end

end

for a = p+1:n

    if Vjnew(a) < Vtip

      m2 = a;

         break;

    end
end

Vjnew2(1) = Vtip;
Vjnew2(2) = Vtip;

Xn(n+1) = Xn(n)+1;
t0(n+1) = t0(n)+1;

for a = 1:n

r(a) = abs(((linerlenght/(n*cos(pi/4))*L)/((t0(a+1)-t0(a))*Vjnew(a)+Xn(a)-
Xn(a+1))));

     tb(a) = 2.92*(r(a)/Vpl);

end

j=2;

    syms U1
    assume(4>U1>0);
    eqn = 0.5.*RoT.*(Ucut.^2)-0.5.*RoP.*(U1-Ucut).^2+Rt-Yp == 0;
    U1 = solve(eqn,U1);
    U1 = max(vpa(U1,5));
```

```
for a = 3:(n-m2)

    if U1 < Vjnew(a-2+m2) & t0(a-2+m2)+t(a-2+m2) < ((SS-Xn(m1))/Vtip)

        j=j+1;

         if Vjnew(a-2+m2) < 0

            Vjnew(a-2+m2) = abs(Vjnew(a-2+m2));

         end

        Vjnew2(a) = Vjnew(a-2+m2);
        tb2(a) = tb(a-2+m2);

    end
end

Xn(j+1) = Xn(j)+1;

Xn2(1) = ((t(m2+j)-t(m1)+(t0(m2+j)-t0(m1))))*Vtip+Xn(m1);
Xn2(2) = ((t(m2+j)-t(m2)+(t0(m2+j)-t0(m2))))*Vtip+Xn(m2);

for a = 3:j

   Xn2(a) = ((t(m2+j)-t(m2+a-2)+(t0(m2+j)-t0(m2+a-2))))*Vjnew2(a)+Xn(m2+a-
2);

end

B(1,1) = Xn2(1);
B(2,1) = Xn2(2);
B(1,2) = Vjnew2(1);
B(2,2) = Vjnew2(2);
B(1,3) = tb(1);
B(2,3) = tb(2);


for a = 3:j

  B(a,1) = Xn2(a);
  B(a,2) = Vjnew2(a);
  B(a,3) = tb2(a);

end
```

```
Pent = 0;

%%%%%%%%%%Jet Tip Penetration%%%%%%%%%%

    syms U
    assume(4>U>0);
    eqn = 0.5.*RoT.*(U.^2)-0.5.*RoP.*((B(1,2))-U).^2+Rt-Yp == 0;
    U = solve(eqn,U);
    U = vpa(U,5);

    if U < 0 | U > B(1,2)

        U = 0;

    end

    if U > Ucut

       pene = (sqrt(RoP/RoT)*(B(1,1)-B(2,1)))*(1-(AA/(B(a,2)).^2));

        if pene > 0

              Pent = Pent+(pene)
        end

     end

%%%%%%%%%%% Jet Tip Penetration %%%%%%%%%%%

SS = SS+Pent;

for a = 2:j

    Rn1(a) = Xn2(a)-Xn2(a-1);

end

for a = 1:(j-1)

   C(a,1) = B(a+1,1);
   C(a,2) = B(a+1,2);
   C(a,3) = B(a+1,3);
```

```
end

Xn2(j+1) = Xn2(j)+1;
C = sortrows(C,1);
j = j-1;

td = 1.7; %Time for the detonation wave to reach the liner at the symmetry
        %axis. The value is taken from the AUTODYN simulations.
tn2 = t(j)+t0(j);
tc = tn2+td

E = C;
E = sortrows(E,1,'descend');
tc2 = tc;

for a = 1:j-1

   Rn2(a) = E(a,1)-E(a+1,1);
   E(a,4) =  Rn2(a);
end

Lfailure = abs((Rn2(j-3)+Rn2(j-4))/2*1.2)
j

%-----------------------------1st Group Penetration-------------------------

F = E;

F(1,1) = 1;
x=1;
i=1;
Pen = 0;
syms U
x = 0;

Pen = Pen+Pent

while i < j-2

   x = x+1;
   tc2 = tc2+ts;
   %F(a,5) = tc;
   F = sortrows(F,1,'descend');
   G = F;
   tc2
```

```
for a = 2:j

    F(a-1,1) = (ts)*F(a-1,2)+F(a-1,1);

end


for a = 2:(j-2)

   if F(a-1,4) == 0

      continue;
   end

   Y = F(a-1,1)-F(a,1);

         if F(a-1,1) > (SS+Pen)

            syms U
            assume(4>U>0);
            eqn = 0.5.*RoT.*(U.^2)-0.5.*RoP.*((F(a,2))-U).^2+Rt-Yp == 0;
            U = solve(eqn,U);
            U = max(vpa(U,5));


            pene = (sqrt(RoP/RoT)*(F(a-1,4)))*(1-(AA/(F(a-1,2))^2));
            i = i+1

               if pene > 0 & pene < Lfailure

                  tt = pene/U;
                  VV = (F(a,2)+U)/2;
                  XX = (F(a+1,2)-VV)*tt;
                  F(a,4) = F(a,4)-XX;

                  Pen = vpa(Pen+pene)

               elseif    pene > Lfailure

                 Pen = vpa(Pen+Lfailure)

               else

               end
```

```
                F(a-1,1) = 0;
                F(a-1,2) = 0;
                F(a-1,3) = 0;
                F(a-1,4) = 0;
            end

        end

end
   F = sortrows(F,1);
   tc = tc2;
   vpa(Pen,3)
   jj=0;

   for a = (m2+j+1):(n)

    if U1 < Vjnew(a) & t0(a)+t(a)-t0(m2+j+1)-t(m2+j+1) < ((SS+Pen-
Xn(m2+j+1))/Vjnew(m2+j+1))

        jj=jj+1;

         if Vjnew(a) < 0

            Vjnew(a) = abs(Vjnew(a));

         end

        Vjnew2(a) = Vjnew(a);
        tb2(a) = tb(a);

    end
end

if jj == 0

   vpa(Pen,3)
   Penny(bb) = vpa(Pen,3);
   vpa(Penny,3)

end

Xn(j+1) = Xn(j)+1;

for a = m2+j+1:m2+j+jj
```

```
    Xn2(a) = ((t(m2+j+jj)-t(a)+(t0(m2+j+jj)-t0(a))))*Vjnew2(a)+Xn(a);

end

for a = 1:jj

   H(a,1) = Xn2(a+(m2+j));
   H(a,2) = Vjnew2(a+(m2+j));
   H(a,3) = tb2(a+(m2+j));

end

jj = jj-1;

I = H;
I = sortrows(I,1,'descend');
I(1,1)=0;

for a = 1:jj

    Rn3(a) = I(a,1)-I(a+1,1);
    I(a,4) =  Rn3(a);

    if I(a,2)<0.5

        jj=jj-1;

    end
end

if jj > 3
Lfailure = abs((Rn3(jj-5)+Rn3(jj-7))/2*1.2);

else

Lfailure = 7.5*10/n;

end

%-------------------------2nd Group Penetration----------------------------

J = I;
J(1,1) = 1;
ii=0;
```

```
while ii < jj-2

    x = x+1;
    tc2 = tc2+ts;
    J = sortrows(J,1,'descend');
    tc2;

    for a = 2:jj

        J(a-1,1) = (ts)*J(a-1,2)+J(a-1,1);

    end


    for a = 2:(jj-2)

       if J(a-1,4) == 0

          continue;
       end

       Y = J(a-1,1)-J(a,1);

            if J(a-1,1) > (SS+Pen)

                syms U
                assume(4>U>0);
                eqn = 0.5.*RoT.*(U.^2)-0.5.*RoP.*((J(a,2))-U).^2+Rt-Yp == 0;
                U = solve(eqn,U);
                U = max(vpa(U,5));

                pene = (sqrt(RoP/RoT)*(J(a-1,4)))*(1-(AA/(J(a-1,2))^2));
                ii = ii+1

                if ii == 1

                   tc2 = tc; % time correction

                end

                   if pene > 0 && pene < Lfailure

                      Pen = vpa(Pen+pene)
```

```
                tt = pene/U;
                VV = (J(a,2)+U)/2;
                XX = (J(a+1,2)-VV)*tt;
                J(a,4) = J(a,4)-XX;


            elseif    pene > Lfailure

              Pen = vpa(Pen+Lfailure/2)

            else

            end

          J(a-1,1) = 0;
          J(a-1,2) = 0;
          J(a-1,3) = 0;
          J(a-1,4) = 0;
        end

    end

end
   I = sortrows(I,1);
   tc2; %Total penetration time (μs)
   vpa(Pen,3)
```